Mechanism of Chorismate Mutase: Contribution of Conformational Restriction to Catalysis in the Claisen Rearrangement

Nikolai A. Khanjin, James P. Snyder, and F. M. Menger*

Contribution from the Department of Chemistry, Emory University, Atlanta, Georgia 30322

Received July 12, 1999

Abstract: The mechanism of the enzyme- and antibody-catalyzed Claisen rearrangement of chorismate to prephenate was investigated experimentally on model compounds and by using quantum chemistry calculations at the Becke3LYP/6-31G* level of theory. Conformational restriction of the allyl vinyl ether fragment to the reactive chairlike conformation in **1** induces a 2×10^5-fold rate acceleration ($\Delta\Delta G^{\ddagger} = 7.3$ kcal/mol) of the Claisen rearrangement in C_6D_6 relative to an unrestricted analogue **3**. A direct relationship between activation barrier lowering and the distance between reactive termini has been observed in additional model systems. Compression of the reactive centers from 4.0 to 3.0 Å results in a barrier lowering from 24 kcal/mol to 12 kcal/mol in one conformationally restricted model. Further compression reduces the activation barrier to a mere 4 kcal/mol. Rearrangement rate increases via conformational restriction and reactive center compression derive mainly from ground-state destabilization in which entropic factors do not contribute significantly. The chorismate mutase mechanism is rationalized as a series of three steps involving (1) capture of the unstable pseudo-diaxial conformer of chorismate in a chairlike geometry (<3 kcal/mol contribution to barrier lowering); (2) further confinement of the reacting termini with a potential for >10 kcal/mol barrier reduction; and (3) rearrangement accompanied by additional transition-state stabilization from ionic H-bonding at the ether oxygen. Since the total barrier lowering is greater than that required to account for the observed 3×10^6-fold enzymatic catalysis, the rearrangement itself is probably not the rate-determining step. The major contribution to catalysis could, in principle, come from confining the reactive centers to contact distances, a conclusion consistent with the spatiotemporal precept.

Introduction

Chorismate mutase promotes a 3×10^6-fold rate acceleration of the Claisen rearrangement of chorismate into prephenate (Scheme 1).[1,2] This key step in the shikimate biosynthetic pathway furnishes aromatic amino acids as well as other biologically important aromatic compounds.[3] Since the pathway exists only in organisms such as bacteria, fungi, and higher plants, its inhibitors and substrate analogues are possible leads to novel antibiotics, fungicides, and herbicides.[4] Thus, the elucidation of chorismate mutase's mode of action has important practical ramifications. In addition to pharmacological relevance, chorismate mutase enjoys the distinction of being the only fully characterized enzyme that catalyzes a pericyclic reaction[5,6] (neglecting the recently isolated "Diels−Alder-ase"[7] and catalytic antibodies for the oxy-Cope rearrangement[8]). Pericyclic reactions are generally known as simple, one-step processes unencumbered by intermediates. In contrast to many enzyme-catalyzed reactions, the corresponding nonenzymatic process proceeds smoothly and can therefore be used directly for comparison purposes. Thus, the enzyme embodies features that

Scheme 1

make it particularly attractive for mechanistic investigation and for elaborating general principles of enzyme catalysis.

X-ray structures of the enzymes from *Bacillus subtilis* (BsCM),[9] *Escherichia coli*,[10] and yeast[11−13] have been elucidated (Figure 1). Despite the poor sequence homology, the active sites of the three proteins are very similar. Near perfect complementarity at hydrophobic, polar, and ionic centers is displayed by the transition-state analogue (TSA) and the active site. Further-

(1) Review: Ganem, B. *Angew. Chem., Int. Ed. Engl.* **1996**, *35*, 937−945.

(2) Review: Lee, A. Y.; Stewart, J. D.; Clardy, J.; Ganem, B. *Chem. Biol.* **1995**, *2*, 195−203.

(3) Review: Dewick, P. M. *Nat. Prod. Rep.* **1998**, *15*, 17−58.

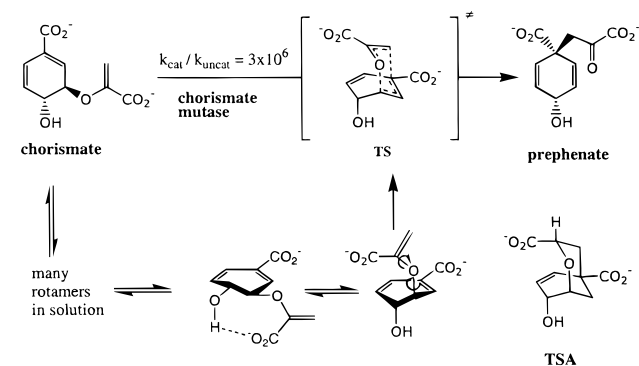(4) Review: Haslam, E. *Shikimic Acid Metabolism and Metabolites*; John Wiley & Sons: New York, 1993.

(5) Pindur, U.; Schneider, G. H. *Chem. Soc. Rev.* **1994**, *23*, 409−415.

(6) Laschat, S. *Angew. Chem., Int. Ed. Engl.* **1996**, *35*, 289−291.

(7) Ichihara, A.; Oikawa, H. *Biosci., Biotechnol., Biochem.* **1997**, *61*, 12−18.

(8) Ulrich, H. D.; Mundroff, E.; Santarsiero, B. D.; Driggers, E. M.; Stevens, R. C.; Schultz, P. G. *Nature (London)* **1997**, *389*, 271−275.

(9) Chook, Y. M.; Gray, J. V.; Ke, H.; Lipscomb, W. N. *J. Mol. Biol.* **1994**, *240*, 476−500.

(10) Lee, A. Y.; Karplus, P. A.; Ganem, B.; Clardy, J. *J. Am. Chem. Soc.* **1995**, *117*, 3627−3628.

(11) Sträter, N.; Schnappauf, G.; Braus, G.; Lipscomb, W. N. *Structure (London)* **1997**, *5*, 1437−1452.

(12) Xue, Y.; Lipscomb, W. N.; Gray, R.; Schnappauf, G.; Braus, G. *Proc. Natl. Acad. Sci. U.S.A.* **1994**, *91*, 10814−10818.

(13) Sträter, N.; Håkansson, K.; Schnappauf, G.; Braus, G.; Lipscomb, W. N. *Proc. Natl. Acad. Sci. U.S.A.* **1996**, *93*, 3330−3334.
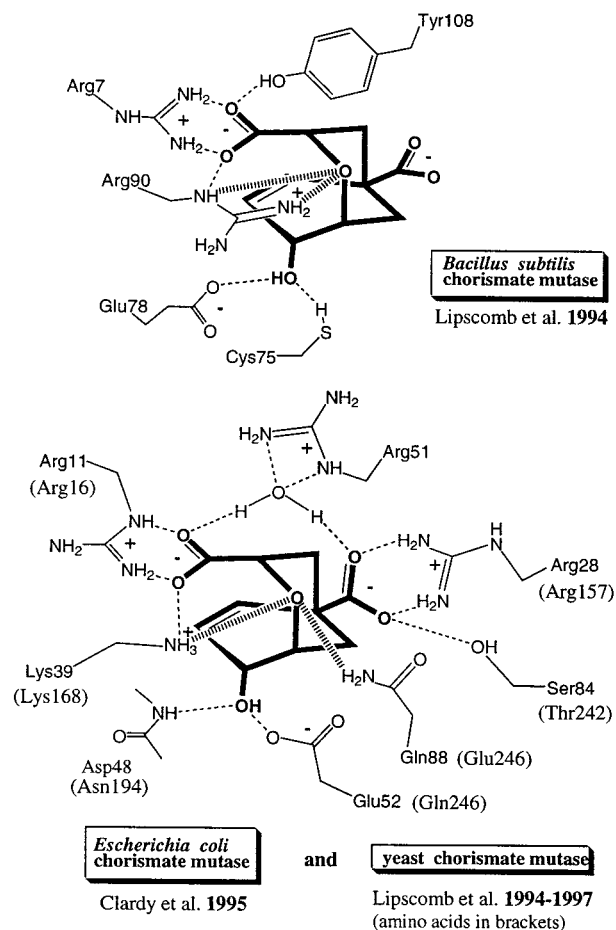
Figure 1. Polar interactions with inhibitor at the active sites of three different chorismate mutases obtained from X-ray studies.[3,9–11] According to coordinates for the *B. subtilis* enzyme, deposited with the Protein Data Bank,[9] the position of the Arg63 side chain is not conformationally restricted. The enzyme is trimeric but only one of the units has the Arg63 complexed with a carboxylate as shown.

more, two catalytic antibodies, 1F7[14,15] and 11F1-2E11,[16] have been reported to mimic the enzymes with 250-fold and 10[4]-fold catalytic effects, respectively. The structure of 1F7 has also been established by X-ray crystallography (Figure 2).[14] Both mutase-catalyzed and uncatalyzed rearrangements are believed to proceed via transition states with a chairlike geometry.[17–19] The enzymes and the two abzymes are known to function by imposing a diaxial chairlike conformer upon a substrate that normally prefers a diequatorial conformation (Scheme 1). Indeed, a conformationally restricted endo-oxabicyclic analogue of the diaxial chairlike transition state has been employed as a potent mutase inhibitor.[20–22] It was used both to locate the enzyme active sites (Figures 1, 2) and as a hapten[23] in the preparation of the previously mentioned abzymes.

(14) Haynes, M. R.; Stura, E. A.; Hilvert, D.; Wilson, I. A. *Science (Washington, D.C.)* **1994**, *263*, 646–652.
(15) Shin, J. A.; Hilvert, D. *Bioorg. Med. Chem. Lett.* **1994**, *4*, 2945–2948.
(16) Jackson, D. Y.; Liang, M. N.; Bartlett, P. A.; Schultz, P. G. *Angew. Chem., Int. Ed. Engl.* **1992**, *31*, 182–183.
(17) Sogo, S. G.; Widlanski, T. S.; Hoare, J. H.; Grimshaw, C. E.; Berchtold, G. A.; Knowles, J. R. *J. Am. Chem. Soc.* **1984**, *106*, 2701–2703.
(18) Knowles, J. R. *Pure Appl. Chem.* **1984**, *56*, 1005–1010.
(19) Asano, Y.; Lee, J. J.; Shieh, T. L.; Spreafico, F.; Kowal, C.; Floss, H. G. *J. Am. Chem. Soc.* **1985**, *107*, 4314–4320.
(20) Bartlett, P. A.; Johnson, C. R. *J. Am. Chem. Soc.* **1985**, *107*, 7792–7793.
(21) Bartlett, P. A.; Nakagawa, Y.; Johnson, C. R.; Reich, S. H.; Luis, A. *J. Org. Chem.* **1988**, *53*, 3195–3210.
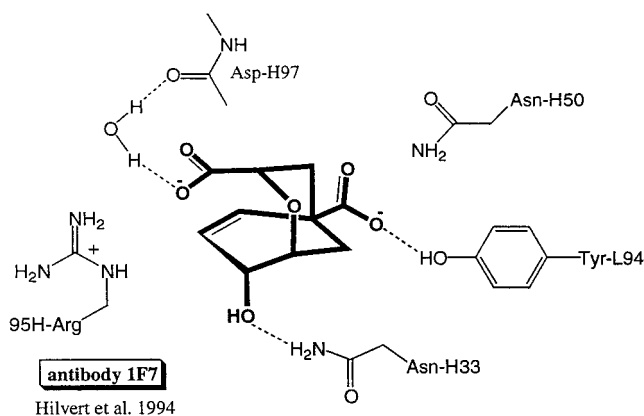

Figure 2. Hydrogen-bonding and electrostatic interactions of the TSA with the active site of 1F7.[14] H-bonds are not shown for residues at distances greater than 3.3 Å from the ligand.

Substrate analogue studies demonstrate that only two carboxylates in the allyl vinyl ether moiety are required for catalysis.[24–30] Kinetic parameters for many chorismate mutases have been obtained (Table 1).[9,31–37] However, interpretation of the kinetic data is uncertain since kinetic isotope effect studies[38,39] demonstrate that the rearrangement itself is not the rate-determining step. Dynamic NMR studies with ^{13}C-labeled prephenate and *B. subtilis* enzyme suggest that the departure of the product from the active site serves as the rate-determining step,[40] implying that the true catalytic effect could be even higher than the observed 3×10^6 value. In addition, site-directed mutagenesis studies on chorismate mutase[3] from *B. subtilis*,[41,42] *E. coli* P-protein,[35,43,44] and *E. coli* T-protein[45,46] reveal the importance of positive charges, as provided by Arg or Lys,

(22) Clarke, T.; Stewart, J. D.; Ganem, B. *Tetrahedron* **1990**, *46*, 731–748.
(23) Mader, M. M.; Bartlett, P. A. *Chem. Rev. (Washington, D.C.)* **1997**, 12811–1301.
(24) Pawlak, J. L.; Padykula, R. E.; Kronis, J. D.; Aleksejczyk, R. A.; Berchtold, G. A. *J. Am. Chem. Soc.* **1989**, *111*, 3374–3381.
(25) Delany, J. J., III; Padykula, R. E.; Berchtold, G. A. *J. Am. Chem. Soc.* **1992**, *114*, 1394–1397.
(26) Delany, J. J., III; Berchtold, G. A. *J. Org. Chem.* **1988**, *53*, 3262–3265.
(27) Lesuisse, D.; Berchtold, G. A. *J. Org. Chem.* **1988**, *53*, 4992–4997.
(28) Pawlak, J. L.; Berchtold, G. A. *J. Org. Chem.* **1988**, *53*, 4063–4069.
(29) Wood, H. B.; Buser, H.-P.; Ganem, B. *J. Org. Chem.* **1992**, *57*, 178–184.
(30) Galopin, C. C.; Ganem, B. *Bioorg. Med. Chem. Lett.* **1997**, *7*, 2885–2886.
(31) Andrew, P. R.; Smith, G. D.; Young, I. G. *Biochemistry* **1973**, *12*, 3492–3498.
(32) Kast, P.; Asif-Ullah, M.; Hilvert, D. *Tetrahedron Lett.* **1996**, *37*, 2691–2694.
(33) Görich, H. *Biochemistry* **1978**, *17*, 3700–3705.
(34) MacBeath, G.; Kast, P.; Hilvert, D. *Biochemistry* **1998**, *37*, 10062–10073.
(35) Galopin, C. C.; Zhang, S.; Wilson, D. B.; Ganem, B. *Tetrahedron Lett.* **1996**, *37*, 8675–8678.
(36) Hilvert, D.; Carpenter, S. H.; Nared, K. D.; Auditor, M.-T. M. *Proc. Nat. Acad. Sci. U.S.A.* **1988**, *85*, 4953–4955.
(37) Jackson, D. Y.; Jacobs, J. W.; Sugaswara, R.; Reich, S. H.; Bartlett, P. A. *J. Am. Chem. Soc.* **1988**, *110*, 4841–4842.
(38) Guilford, W. J.; Copley, S. D.; Knowles, S. D. *J. Am. Chem. Soc.* **1987**, *109*, 5013–5019.
(39) Addadi, L.; Jaffe, E. K.; Knowles, J. R. *Biochemistry* **1983**, *22*, 4494–4501.
(40) Gray, J. V.; Eren, D.; Knowles, J. R. *Biochemistry* **1990**, *29*, 8872–8878.
(41) Cload, S. T.; Liu, D. R.; Pastor, R. M.; Schultz, P. G. *J. Am. Chem. Soc.* **1996**, *118*, 1787–1788.
(42) Kast, P.; Asif-Ullah, M.; Jiang, N.; Hilvert, D. *Proc. Natl. Acad. Sci. U.S.A.* **1996**, *93*, 5043–5048.
(43) Zhang, S.; Kongsaeree, P.; Clardy, J.; Wilson, D. B.; Ganem, B. *Bioorg. Med. Chem.* **1996**, *4*, 1015–1020.

Table 1. Rate Parameters for Chorismate to Prephenate Rearrangement Catalyzed by Proteins

source of reaction, conditions	k_{cat}/k_{uncat}	k_{cat} (s^{-1})	K_m (μM)	K_i (TSA) (μM)	$\Delta H^{\ddagger}$ (kcal/mol)	$\Delta S^{\ddagger}$ (eu)	$\Delta G^{\ddagger}$ (kcal/mol)
uncatalyzed, pH 7.5[9,31]	1				20.5	−12.9	24.2
B. subtilis[9,32]	2 × 10^6	50	100	3	12.7	−9.1	15.4
E. coli T protein[9]	2 × 10^6	72	40	0.3			
Klebsiella pneumoniae[a 9,32,33]	3 × 10^6	13.5	290	0.15	15.9	0.0	15.9
Methanococcus jannaschii[34]	>10^6	5.7	41		16.2	−1.7	
Streptomyces aureofaciens[33]					14.5	−1.6	15.0
Saccharomyces cerevisiae[11]	modulated by 10-fold activation by tryptophan and 10-fold inhibition by tyrosine						
E. coli wild type, pH 7.8[35]					16.3	−3.0	
E. coli (Q88E), pH 4.5[35]					16.6	0.2	
antibody 1F7[9,32,36]	250	0.0012	260	0.6	15.0	−22.0	21.3
antibody 11F1−2E11[9,32,37]	10^4	0.045	51	9	18.3	−1.2	18.7

[a] Old name: *Aerobacter aerogenes*.

placed near the pyruvyl carboxylate and the ether oxygen of the bound ligand.

Claisen rearrangements[47−51] and other 3,3 sigmatropic shifts are both substituent- and charge-sensitive (e.g. anionic oxy-Cope,[52,53] 2-azonium Cope,[53] and Lewis acid-catalyzed Claisen rearrangements[53,54]). Furthermore, the Claisen rearrangement is moderately accelerated (up to 300-fold) in polar solvents and especially in H-bonding media.[1] Ground-state strain destabilization in addition to conformational restriction near the transition-state geometry can lead to a barrier lowering in Cope rearrangements 35−40 kcal/mol for unrestricted acyclic systems to 3−7 kcal/mol in bullvalene, barbaralane, and semibullvalene-like systems. The theoretical possibility exists for achieving a zero barrier in the so-called neutral homoaromatic compounds based on degenerate Cope systems.[55] Finally, the enzyme mechanism has been a subject of many recent computational modeling studies.[56−60]

Analysis of all known information about the enzyme and related systems rules out possible chemical mechanisms such as general acid/base catalysis or nucleophilic/electrophilic participation. Instead, the data point to conformational restriction and further stabilization of the transition state by strong

H-bonding especially to the ether oxygen.[1,2,9,56−59] The purpose of this research was to estimate the contribution of these two factors in the million-fold enzymatic acceleration using model compounds that mimic interactions at the active site. Both experimental and theoretical approaches have been employed. Particular attention was paid to the spatiotemporal guideline[61,64] that predicts a large rate acceleration if the reactive termini in chorismate are held at short contact distances within the active site.[65] In this paper we discuss the relationship between the geometry of the reactant and the rate of Claisen rearrangement with emphasis on rate−distance relationships. The effect on chorismate mutase catalysis of selective transition-state stabilization via electrostatic interactions and strong H-bonding will be discussed in a separate paper.[66]

Results and Discussion

Theoretical Considerations and the Spatiotemporal Principle. Several factors that may contribute to rate accelerations in enzymes have been proposed: proximity, propinquity, approximation, orbital steering, and entropy trapping, among others.[67] All of these notions appeal to "geometry" as their fundamental underpinning. To place "geometry" on a somewhat more quantitative footing than is possible with concepts such as "proximity", it was proposed that the distance between reacting centers be employed to analyze intramolecular and enzymatic reactivity. This simple idea, embodied in the "spatiotemporal principle", states the following: fast reactions between two functionalities are achieved when the reacting centers are held at "contact distances" either by a covalent framework (in the case of intramolecular systems) or by noncovalent forces (in the case of enzymes). "Contact" refers to atomic separations too small to permit intervening solvent. The concept resembles the oft-cited "proximity" effect except that "proximity" is virtually never defined in terms of geometry. The spatiotemporal principle, on the other hand, states that rate accelerations of >10^8 are possible when, for example, a nucleophile is positioned <3 Å above a carbonyl prior to addition. Among other supporting evidence, it was found that a carboxyl properly located near an aliphatic amide induces rapid

(44) Liu, D. R.; Cload, S. T.; Pastor, R. M.; Schultz, P. G. *J. Am. Chem. Soc.* **1996**, *118*, 1789−1790.

(45) Christendat, D.; Saridakis, V. C.; Turnbull, J. L. *Biochemistry* **1998**, *37*, 15703−15712.

(46) Christendat, D.; Turnbull, J. *Biochemistry* **1996**, *35*, 4468−4479.

(47) Wipf, P. In *Claisen Rearrangements* in *Comprehensive Organic Synthesis*; Paquette, L. A., Ed.; Pergamon Press: New York, 1991; Vol. 5, pp 827−873.

(48) Gajewski, J. J.; Jurayj, J.; Kimbrough, D. R.; Gande, M. E.; Ganem, B.; Carpenter, B. E. *J. Am. Chem. Soc.* **1987**, *109*, 1170−1186.

(49) Burrows, C. J.; Carpenter, B. K. *J. Am. Chem. Soc.* **1981**, *103*, 6983−6984.

(50) Coates, R. M.; Rogers, B. D.; Hobbs, S. J.; Peck, D. R.; Curran, D. P. *J. Am. Chem. Soc.* **1987**, *109*, 1160−1170.

(51) Gajewski, J. J.; Gee, K. R.; Jurayj, J. *J. Org. Chem.* **1990**, *55*, 1813−1822.

(52) Hill, R. K. In *Cope, Oxy-Cope and Anionic Oxy-Cope Rearrangements* in *Comprehensive Organic Synthesis*; Paquette, L.A., Ed.; Pergamon Press: New York, 1991; Vol. 5, pp 786−826.

(53) Miller, B. *Advanced Organic Chemistry: Reactions and Mechanisms*, Prentice-Hall: Upper Saddle River, 1998.

(54) Maruoka, K.; Saito, S.; Yamamoto, H. *J. Am. Chem. Soc.* **1995**, *117*, 1165−1166.

(55) For a review on homoaromaticity see: Williams, R. V.; Kurtz, H. A. *Adv. Org. Chem.* **1994**, *29*, 273−331.

(56) Lyne, P. D.; Mulholland, A. J.; Richards, W. G. *J. Am. Chem. Soc.* **1995**, *117*, 11345−11350.

(57) Davidson, M.M.; Gould, I. R.; Hillier, I. H. *J. Chem. Soc., Perkin Trans. 2* **1996**, *4*, 525−532.

(58) Wiest, O.; Houk, K. N. *J. Am. Chem. Soc.* **1995**, *117*, 11628−11639, and references therein.

(59) (a) Carlson, H. A.; Jorgensen, W. L. *J. Am. Chem. Soc.* **1996**, *118*, 8475−8484, and references therein. (b) Severance, D. L.; Jorgensen, W. L. *J. Am. Chem. Soc.* **1992**, *114*, 10966−10968.

(60) Kast, P.; Tewari, Y. B.; Wiest, O.; Hilvert, D.; Houk, K. N.; Goldberg, R. N. *J. Phys. Chem. B* **1997**, *101*, 10976−10982.

(61) Menger, F. M. *Acc. Chem. Res.* **1993**, *26*, 206−212.

(62) Menger, F. M. *Biochemistry* **1992**, *31*, 5368−5373.

(63) Menger, F. M. *Organic Reactivity and Geometric Disposition* in *Advances in Molecular Modeling*; JAI Press Inc.: Greenwich, 1988; Vol. 1, pp 189−213.

(64) Menger, F. M. *Acc. Chem. Res.* **1985**, *18*, 128−134.

(65) Menger, F. M.; Nelson, Jr., K. H.; Sherrod, M. J. Relative rates of enzyme- and abzyme-catalyzed rearrangement of chorismate to prephenate. Analysis via computational-based spatiotemporal theory, unpublished results.

(66) Khanjin, N. A.; Snyder, J. P. Manuscript in preparation.

(67) *Enzyme Mechanisms*; Page, M. I., Williams A., Eds.; Royal Society of Chemistry: London, 1987.

amide hydrolysis at pH = 7.0 (22 °C), representing a $>10^8$ catalysis.[68] Numerous other examples illustrate the spatiotemporal principle,[61,64] which resembles traditional ground-state strain explanations of enzymatic and intramolecular reactivity (including desolvation strain) except that distance, rather than energy, is the key parameter.

An important corollary of the spatiotemporal precept particularly relevant to the chorismate mutase problem follows: If the reactive functionalities escape their contact distance by even a single free rotation, the reaction rate can fall precipitously. This proposition departs radically from classical entropy-based theories which claim that creation of a single free rotation diminishes the rate by a mere 5-fold. The above-mentioned 30 kcal/mol drop in activation barrier for the Cope rearrangement by covalent restriction in semibulvallene-like systems is higher than any known enzymatic rate acceleration! However, these systems hardly represent ideal models for chorismate mutase, since it is unclear how the enzyme would create such strained substrates at its active site using weak noncovalent interactions. In this respect, the approximately 10^7-fold acceleration of the Cope rearrangement of **A** and **B** below[69] relative to the unrestricted analogue **C** provides a somewhat better enzyme model. Additional such examples of accelerated Claisen rearrangement could not be found in the literature. Nor can

	A	**B**	**C**
E_a	ca 25 kcal/mol	25.0 kcal/mol	34.2 kcal/mol
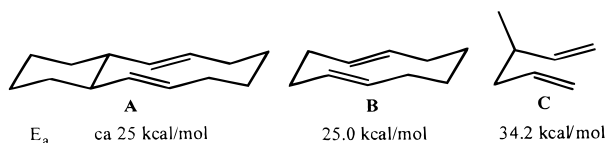
complementarity of the active site to the diaxial conformer account fully for the catalytic rates because the fast enzymes and slow catalytic antibody 1F7 both bind chorismate in the diaxial form. In any event, since a respectable proportion (10−20%) of chorismate exists as the diaxial conformer even in water solution,[70] imposition of a diaxial conformation on the substrate at the active site can explain, at most, only a 10-fold catalysis above background. Entropic destabilization of the ground state by conformational restriction likewise cannot contribute significantly to mutase catalysis.[71,72] At most the enzyme may increase the entropy of the uncatalyzed reaction in water from $\Delta S^{\ddagger} = -12.9$ eu to near 0 eu as found with most chorismate mutases (Table 1). This corresponds to a maximum of 3.8 kcal/mol (at 300 K) or only a 500-fold contribution to the rate increase.

It has also been argued that the Claisen rearrangement of chorismate involves a transition state with polar character. Electrostatic stabilization of the transition state at the active site might, therefore, accelerate the reaction. However, solvent effects on model rearrangements[1,48] are comparatively small (e.g. 11-fold increase from benzene to methanol), so that charge effects probably contribute only modestly to catalysis.

The spatiotemporal model predicts that constraint of chorismate to the reactive chairlike conformation would not cause a significant rate increase (as in case of antibody 1F7) unless the
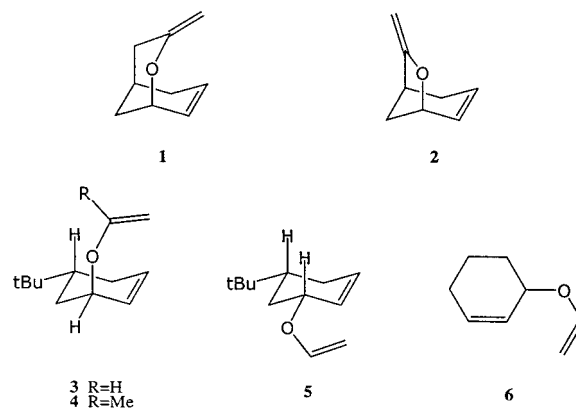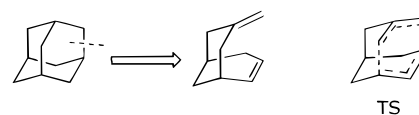
(68) Menger, F. M.; Ladika, M. *J. Am. Chem. Soc.* **1988**, *110*, 6794−6796.
(69) Wharton, P. S.; Johnson, D. W. *J. Org. Chem.* **1973**, *38*, 4117−4121.
(70) Copley, S. D.; Knowles, J. R. *J. Am. Chem. Soc.* **1987**, *109*, 5308−5313.
(71) Page, M. I.; Jencks, W. P. *Proc. Natl. Acad. Sci. U.S.A.* **1971**, *68*, 1678−1683.
(72) Page, M. I.; Jencks, W. P. *Gazz. Chim. Ital.* **1987**, *117*, 455−460.

Figure 3. Compounds synthesized and kinetically studied in this work.

Scheme 2

reactive termini are confined to short distances. The magnitude of catalysis will depend on the time-averaged distance at the active site. As will be shown, the operation of spatiotemporal effects can potentially achieve a catalytic effect in excess of the 3×10^6-fold value manifested by the enzyme.

Design of Compounds. Although the detailed chemical mechanism of an enzyme can be defined only by direct study of the protein itself, enzyme systems are often too complex to permit development of a complete mechanistic picture. Thus, we rely here on a basic understanding of model reactions that mimic certain intramolecular interactions at the active site.

Conformationally rigid 1,5-unsaturated compounds can model conformational restriction of chorismate at the binding site of chorismate mutase. To differentiate the influence of strain and substituent effects from the distance factor on the rate of 3,3 shifts, we attempted to use relatively unstrained nonpolar hydrocarbon skeletons as ground-state models in our work. For example, in principle, restricted 1,5-unsaturated compounds can be generated from unstrained adamantane, diamantane, and decalin skeletons via hypothetical cleavage of a selected σ-bond and introduction of two double bonds in the resulting chairlike cyclohexane fragment as illustrated in Scheme 2. This procedure can be modeled readily with any reliable molecular mechanics program followed by optimization to give a structure with the 1,5-unsaturated fragment restricted to the chairlike geometry required for rearrangement. The skeleton can be extended or shortened, and any carbon can be replaced with a heteroatom, to produce any of a large number of 1,5-unsaturated analogues. In this work we focused on the Claisen substrates shown in Figures 3, 4, and 5. The latter, Figure 5, also records C- - -C termini distances generated by the MM2 force field during initial phases of the study. These suggested a number of novel Claisen substrates with monotonically decreasing C- - -C separation. Subsequent quantum mechanical geometry optimization confirmed the distance dependence.

Compounds **1**−**6** were synthesized and subjected to kinetic analysis. Other structures were studied theoretically at the Becke3LYP/6-31G* level of theory after successful calibration of the computational method with the experimentally studied systems. Bicyclic compound **1** mimics chorismate folded at the active site, whereas analogues **3** and **4** (Figure 3) represent chorismate in solution with unrestricted rotation around the σ-bonds. In model compounds **10**−**14**, the 1,5-unsaturated
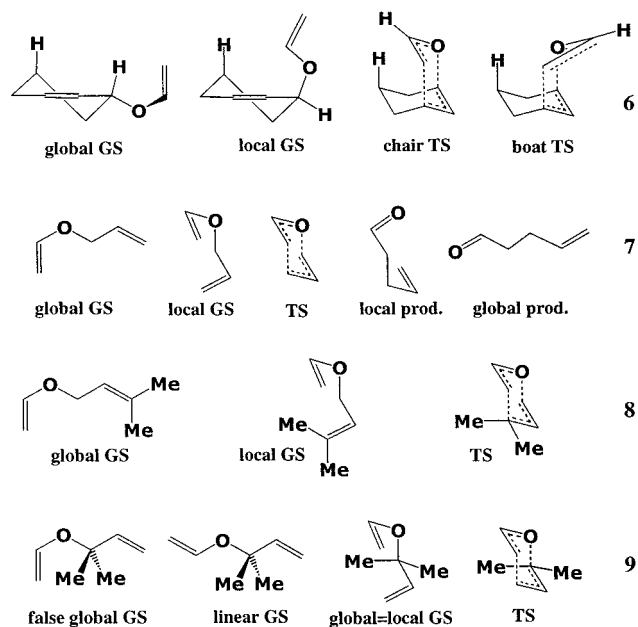
Figure 4. Optimized structures of flexible reactants, Claisen transition states, and products. Global refers to global conformational minima of the reactant (GS) and product (prod); local refers to the minima nearest the transition state.

Figure 5. For the structures treated computationally, Becke3LYP/6-31G* optimized distances between reactive termini are listed beneath the rigid reactants and Claisen transition states. For the local reactant ground states, the corresponding MM2 distances are given in parentheses, as are the NBO bond orders for the transition states. ΔH^*(calc) values were obtained at Becke3LYP/6-31G* geometries.

moiety is constructed similar to **1** in a near perfect chairlike geometry with different distances between the reactive termini.

Scheme 3. Synthesis of **1** and **2**
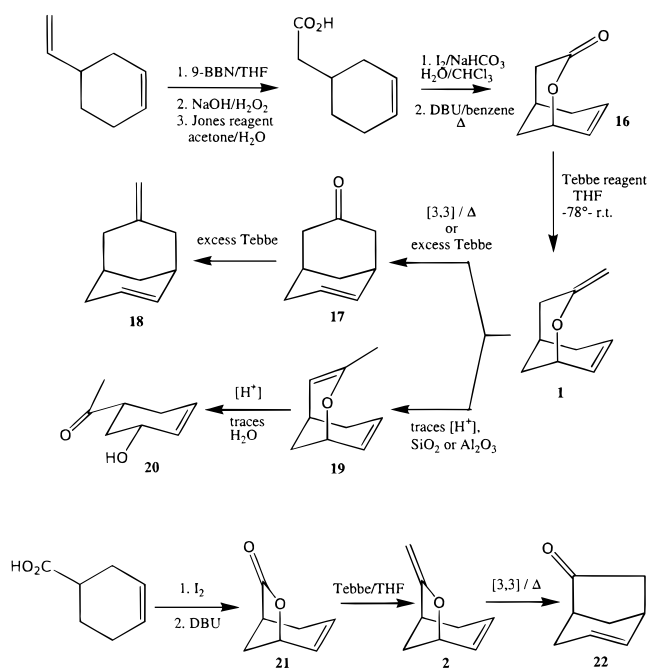
The dependence of activation barriers on distance in these compounds constitutes a test for the spatiotemporal postulate.

Synthesis. The synthesis of **1** is illustrated in Scheme 3. Preparation of bicyclic lactone **16** was carried out according to the literature[73,74] starting from 4-vinylcyclohexene. Conversion of **16** to product **1** via the Tebbe methylenation protocol[75] was troublesome for several reasons. First, if even a slight excess of Tebbe reagent was used, bicyclic diene **18** was isolated as the only product. Presumably, it formed in tandem from Tebbe lactone olefination, Lewis acid-catalyzed Claisen rearrangement of **1**, and Tebbe olefination of intermediate ketone **17**. It has been reported that such a tandem reaction usually requires 3 equiv of Tebbe reagent and proceeds in 12 h.[76] In addition, the desired **1** with an exocyclic double bond underwent acid-catalyzed double-bond migration to form the more stable endo-isomer **19** during workup. For example, in "acid-free" commercial CDCl$_3$ **1** has a half-life of only a few minutes at room temperature, forming **19**, which in turn slowly hydrolyzed to hydroxyketone **20** by the action of traces of water. Isomerization and partial hydrolysis of **1** also occurred during silica and alumina absorption. Only the use of acid-free glassware, excess of lactone **16**, and cold basic alumina filtration with 0.5% Et$_3$N or Me$_3$N in pentane at −78 °C gave the desired product **1**. CDCl$_3$ was specially treated to remove traces of HCl prior to use as an NMR solvent for **1** and our other synthesized vinyl ethers.

The ring-contracted analogue **2** was synthesized using the same protocol (Scheme 3). Vinyl ethers **3**−**5** were prepared from the corresponding *trans*- and *cis-tert*-butyl-cyclohexenols **23** and **25**, the syntheses of which have been described in the literature[77]

(73) Benson, J. A.; Dervan, P. B.; Malherte, R.; Jenkins, J. A. *J. Am. Chem. Soc.* **1976**, *98*, 5937−5969.

(74) Carroll, F. I.; Abraham, P.; Pitner, J. B.; Jablonski, S. D.; Singh, P.; Kwon, Y. W.; Triggle, D. J. *J. Chem. Soc., Chem. Commun.* **1992**, *10*, 795−796.

(75) Pine, S. H.; Kim, G.; Lee, V.; Ruggeri, B.; Heathcock, C. H. In *Organic Syntheses*; John Willey & Sons: New York, 1993; Collect. Vol. VIII, pp 512−515.

(76) Stevenson, J. W. Sam; Bryson, T. A. *Tetrahedron Lett.* **1982**, *23*, 3143−3146.

(77) Chamberlain, P.; Roberts, M. L.; Whitham, G. H. *J. Chem. Soc. B* **1970**, 1374−1381.

Table 2. Rate Parameters for the Claisen Rearrangement of Compounds **1**−**6** and Other Allyl Vinyl Ethers[a]

compound, conditions	T [°C]	Arrhenius parameters T_m [K]	E_a	log A	$\Delta H^{\ddagger}$	$\Delta S^{\ddagger}$ [eu]	$\Delta G^{\ddagger\,b}$	k, rel[b]
1, C$_6$D$_6$	39−75	332	23.5 ± 0.4	11.6 ± 0.3	22.8 ± 0.4	−7.9 ± 1.2	25.18	2.1 × 10^5
1, CDCl$_3$	35−55	318	20.8 ± 1.8	10.3 ± 1.2	20.2 ± 1.8	−13.4 ± 5.5	24.26	9.6 × 10^5
2, C$_6$D$_6$	170, 180			40% side reactions			34.9^d	0.3^d
3, C$_6$D$_6$	139−170	426.6	30.3 ± 1.6	11.2 ± 0.8	29.5 ± 1.6	−10.2 ± 3.8	32.5; 33.6^c	1^{b-d}
3, DMSO-d_6	60, 139		60 °C: no reaction after 35 days				32.64^c	3.2^c
3, DMSO/D$_2$O, 3:1	60, 139		60 °C: no reaction after 35 days				31.96^c	7.4^c
3, DMSO + 3 equiv iPr$_2$NH$_2$Br	60, 139		60 °C, 35 days: 90% ether cleavage; 139 °C, 30 min: 100% ether cleavage					
4, C$_6$D$_6$	120−180	427	30.3 ± 1.8	11.4 ± 1.0	29.5 ± 1.8	−8.9 ± 4.4	32.15	1.89
5, C$_6$D$_6$	110−180	418.8	28.2 ± 1.0	10.6 ± 0.6	27.3 ± 1.0	−12.7 ± 2.5	31.17	9.71
6, C$_6$D$_6$	110−180	418.8	28.2 ± 0.7	10.5 ± 0.4	27.3 ± 0.7	−13.1 ± 1.7	31.29	7.97
7, C$_6$D$_6$[51]	118−153		26.5 ± 0.3	10.3 ± 0.2	25.7 ± 0.3	−14.1 ± 0.6	30.0	68
7, gas phase[79]	155−201	457.8	30.3 ± 0.6	11.6 ± 0.3	29.4 ± 0.6	−8.4 ± 1.3	31.96	2.6
7, Bu$_2$O[83]	113−173				25.4 ± 0.7	−15.9 ± 1.5		
allyl isopropenyl ether, gas[81]	143−194		29.3	11.73		−7.7		
C$_6$D$_6$[51]	80−125		25.7 ± 0.3	10.5 ± 0.2	24.9 ± 0.3	−13.2 ± 0.6		
2-methylallyl vinyl ether, gas[82]	150−188		29.10	11.15		−10.23		
1-methylallyl vinyl ether, gas[80]	117−168		27.87	11.32		−9.45		
in 1-decene[80]	100−145		25.74	10.78		−11.9		
in benzonitrile[80]	84−135		25.30	10.91		−11.33		
1-n-C$_5$H$_{11}$−allyl isopropenyl ether, C$_6$D$_6$[51]	40−79		26.0	11.97	25.3 ± 0.5	−5.97 ± 0.1		
1-methyl-1-n-pentylallyl isopropenyl ether, C$_6$D$_6$[51]	40−76		21.6 ± 0.6	10.70	20.9 ± 0.6	−11.79		

[a] $\Delta H^{\ddagger}$, E_a, $\Delta G^{\ddagger}$ are in kcal/mol. [b] Calculated at 30 °C. [c] At 139 °C. [d] At 180 °C.

Scheme 4. Synthesis of **3**−**5**
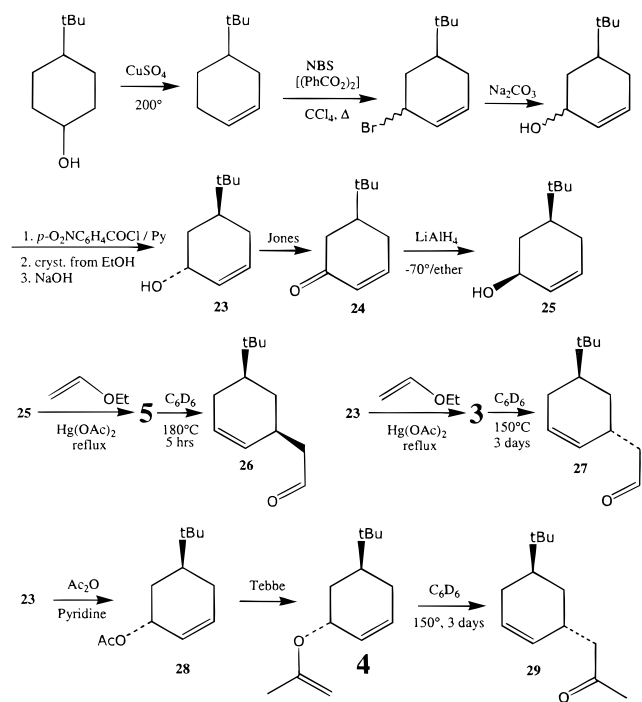
and reproduced as pictured in Scheme 4. The synthesis of **6** and its Claisen rearrangement have been described previously[78] without accompanying kinetic data.

Kinetic Measurements. All compounds gave Claisen rearrangement products in quantitative yields except for **2**, which rearranged with 30−40% side products. Reactions followed a first-order rate law, and the temperature dependence of the rate constants gave linear Arrhenius plots. The results of the kinetic studies are summarized in Table 2. For comparison, published kinetic data for allyl vinyl ethers with aliphatic substituents have been included.[51,79−83]

Conformationally restricted compound **1** rearranges 2 × 10^5 times faster than its unrestricted analogue **3** in benzene-d_6 solution. The rate increase is achieved by a simultaneous lowering of the enthalpy of activation by the relatively large value of 6.7 kcal/mol and a relatively small entropy increase of 2.3 eu. In **1** the geometry of the 1,5-unsaturated fragment is restricted to an ideal chairlike conformation, while in **3** the molecule can escape a reactive chairlike arrangement by rotation around two exocyclic σ-bonds. The third σ-bond in the allyl vinyl ether unit is part of the cyclohexene ring. The bulky *tert*-butyl group locks the torsional angle around this bond into the pseudoequatorial position and thereby forces the vinyl ether substituent into the pseudoaxial orientation required for rearrangement. Thus, simple conformational restriction of the two mobile bonds on going from **3** to **1** leads to a rate increase of 2 × 10^5-fold, the major contribution to the rate acceleration coming from enthalpic effects. The entropy contribution (2.3 eu or 0.7 kcal/mol at 30 °C or 3-fold rate increase) is even smaller than the suggested value of 6−10 eu per two rotations (5−10-fold rate increase per rotation), as estimated by Page and Jencks.[71] The reactive chairlike conformation and chairlike transition state of **3** is destabilized by unfavorable 1,3-diaxial interactions between the vinyl group above the ring and a pseudoaxial hydrogen. In **1** the vinyl fragment is held above the ring by the covalent skeleton. Consequently, such R/H 1,3-diaxial interactions are absent.

Although **2** is also conformationally restricted and possesses the same distance between reactive termini as does **1** (ca. 4.0 Å), the allyl vinyl ether fragment is not in an ideal chairlike conformation, resulting in a 7 × 10^5 rate decrease relative to **1**. Addition of a methyl group to the vinyl ether in **4** caused no change in the $\Delta H^{\ddagger}$ compared to **3**, but gave instead a small $\Delta S^{\ddagger}$ increase of 1.3 eu (i.e., −10.2 eu in **3** and −8.9 eu in **4**), which

(78) Burgstahler, A. W.; Nordin, I. C. *J. Am. Chem. Soc.* **1961**, *83*, 198−206.

(79) Schuler, F. W.; Murphy, G. W. *J. Am. Chem. Soc.* **1950**, *72*, 3155−3159.

(80) Frey, H. M.; Montague, D. C. *Trans. Faraday Soc.* **1968**, *64*, 2369−2374.

(81) Stein, L.; Murphy, G. W. *J. Am. Chem. Soc.* **1952**, *74*, 1041−1043.

(82) Frey, H. M.; Pope, B. M. *J. Chem. Soc. B* **1966**, 209−210.

(83) Burrows, C. J.; Carpenter, B. K. *J. Am. Chem. Soc.* **1981**, *103*, 6983−6984.

Mechanism of Chorismate Mutase

J. Am. Chem. Soc., Vol. 121, No. 50, 1999 11837

might be associated with an increase in the rotational barrier around vinyl−O bond. Compound **5**, the *cis*-isomer of **3**, rearranges 9.7 times faster than **3** despite confinement of the vinyl ether substituent to the unfavorable pseudoequatorial position. The 3-cyclohexenyl vinyl ether **6** displays activation parameters almost identical to those for **5**, suggesting a similarity in the geometry of ground and transition states for these two compounds.

Compound **3** exhibited small rate increases of 3.2- and 7.4-fold when the solvent was changed from nonpolar benzene to DMSO and DMSO/H_2O, respectively. **1** in chloroform gave a rate increase of 4.6-fold relative to benzene. The latter small rate acceleration can be attributed to weak H-bond stabilization of the transition state by chloroform, which lowers $\Delta H^{\ddagger}$ by 2.6 kcal/mol and $\Delta S^{\ddagger}$ by −5.5 eu relative to benzene.

Note that the reactive termini in **1** are separated by almost 4.0 Å, which is larger than the sum of terminal carbon van der Waals radii of 3.4 Å. Thus, we can expect much larger rate accelerations for compounds **10**−**14**, which are calculated to have contact distances ≤ 3.4 Å (Figure 5). Experimental studies were limited, however, by our ability to readily synthesize the compounds. Furthermore, experimentally derived activation parameters cannot provide information about the geometry and electronic structure of the reactants and transition states nor give a full description of the reaction pathways. Thus, we felt it necessary to apply theoretical methods to the problem. Below we describe a computational protocol that reproduces our experimental activation parameters, and then we apply it to the experimentally inaccessible substrates.

DFT Calculations. The Becke3LYP/6-31G* level of theory[84] as implemented in Gaussian 94 and 98 was used to obtain optimized geometries of reactants and transition states, relative energies, and reaction pathway properties.[85,86] To assess activation barriers for flexible molecules, we performed Monte Carlo conformational searches using the MM3* force field with MacroModel,[87] followed by geometry optimization of the presumptive global minima with the Gaussian series of programs. This provided an estimate of $\Delta H^{\ddagger}$ or E_a. The prediction of entropies for conformationally flexible structures from frequency analysis is limited, because Gaussian treats all $3N-6$ internal degrees of freedom as vibrations by default.[88] Although low-frequency molecular movements such as internal rotations

and ring puckering modes contribute significantly to the entropy and should be treated separately for quantitative predictions,[89] we found the entropy estimates from frequency analysis to be in satisfactory qualitative agreement with the experiment.

Molecular structures on which we performed calculations are shown in Figures 4 and 5. Tables 3 and 4 summarize calculated energies, entropies, and activation parameters as well as bond distances and bond orders (BO) for the reacting bonds. BO were computed according to the Wiberg method implemented in the NPA/NBO facility in Gaussian.[90]

Computational Analysis of the Parent Claisen Rearrangement. A detailed investigation of the parent Claisen rearrangement of allyl vinyl ether was performed. Monte Carlo conformational searching with the MM3* force field in MacroModel generated 14 conformations. None resemble a chairlike geometry. The global minimum and the conformer nearest to a chairlike local minimum were both optimized with Becke3LYP/6-31G*. The optimized geometries and relative energy ($\Delta H = 1.3$ kcal/mol) did not deviate significantly from the MM3* values. A chairlike Becke3LYP/6-31G* Claisen transition state was located from the initially generated guess structure by computing approximate frequencies with G-94 followed by the default transition state (TS) optimization. Frequency analysis of the refined transition structure in combination with intrinsic reaction coordinate (IRC) calculations[91] allowed us to calculate the minimum energy reaction pathway (MEP) from the TS to the nearest the local minima, allyl vinyl ether and 4-pentenal. Conformational features of the latter are identical to the local minima generated from the initial MM3* guess.

The Becke3LYP/6-31G* $\Delta H^{\ddagger} = 27.2$ kcal/mol for rearrangement of allyl vinyl ether is in satisfactory agreement with the experimental values of $\Delta H^{\ddagger} = 29.4$ and 25.7 kcal/mol for the gas-phase and benzene solution transformations, respectively. However, our $(\Delta E + ZPE)^{\ddagger} = 27.7$ kcal/mol is in minor disagreement with the previously obtained value of 26.8 kcal/mol using the same level of theory.[92] Since both calculations yield identical TS energies and structures, the difference lies in the identification of the global minimum for allyl vinyl ether. The Monte Carlo conformational search has definitely located a lower energy global minimum (Figure 4).

Predicted activation parameters for various other levels of theory are summarized in Table 4.[92−95] Clearly, the Becke3LYP method is superior to other DFT methods (BLYP and SVWN) and MP2, all of which include contributions to electron correlation effects. The HF procedure overestimates E_a by 60%, but nonetheless generates a transition structure similar to Becke3LYP. In the latter transition state, **7-TS**, the C−O bond (1.904 Å) is 51% broken, while the new C−C bond (2.314 Å) is only 33% formed as estimated by NBO bond orders (Table 3). This result is in agreement with bond scission values of 50−70% and 10−30%, respectively, obtained from experimental measurement of heavy-atom isotope effects.[96]

(84) Becke, A. D. *J. Chem. Phys.* **1993**, *98*, 5648−5652.

(85) Frisch, M. J.; Trucks, G. W.; Schlegel, H. B.; Gill, P. M. W.; Johnson, B. G.; Robb, M. A.; Cheeseman, J. R.; Keith, T.; Petersson, G. A.; Montgomery, J. A.; Raghavachari, K.; Al-Laham, M. A.; Zakrzewski, V. G.; Ortiz, J. V.; Foresman, J. B.; Cioslowski, J.; Stefanov, B. B.; Nanayakkara, A.; Challacombe, M.; Peng, C. Y.; Ayala, P. Y.; Chen, W.; Wong, M. W.; Andres, J. L.; Replogle, E. S.; Gomperts, R.; Martin, R. L.; Fox, D. J.; Binkley, J. S.; Defrees, D. J.; Baker, J.; Stewart, J. P.; Head-Gordon, M.; Gonzalez, C.; Pople, J. A. *Gaussian 94*, revision D.3; Gaussian, Inc.: Pittsburgh, PA, 1995.

(86) Frisch, M. J.; Trucks, G. W.; Schlegel, H. B.; Scuseria, G. E.; Robb, M. A.; Cheeseman, J. R.; Zakrzewski, V. G.; Montgomery, J. A., Jr.; Stratmann, R. E.; Burant, J. C.; Dapprich, S.; Millam, J. M.; Daniels, A. D.; Kudin, K. N.; Strain, M. C.; Farkas, O.; Tomasi, J.; Barone, V.; Cossi, M.; Cammi, R.; Mennucci, B.; Pomelli, C.; Adamo, C.; Clifford, S.; Ochterski, J.; Petersson, G. A.; Ayala, P. Y.; Cui, Q.; Morokuma, K.; Malick, D. K.; Rabuck, A. D.; Raghavachari, K.; Foresman, J. B.; Cioslowski, J.; Ortiz, J. V.; Stefanov, B. B.; Liu, G.; Liashenko, A.; Piskorz, P.; Komaromi, I.; Gomperts, R.; Martin, R. L.; Fox, D. J.; Keith, T.; Al-Laham, M. A.; Peng, C. Y.; Nanayakkara, A.; Gonzalez, C.; Challacombe, M.; Gill, P. M. W.; Johnson, B. G.; Chen, W.; Wong, M. W.; Andres, J. L.; Head-Gordon, M.; Replogle, E. S.; Pople, J. A. *Gaussian 98*, revision A.3; Gaussian, Inc.: Pittsburgh, PA, 1998.

(87) MacroModel V4.5: Mohamadi, F.; Richards, N. G. J.; Guida, W. C.; Liskamp, R.; Caufield, C.; Chang, G.; Hendrickson, T.; Still, W. C. *J. Comput. Chem.* **1990**, *11*, 440.

(88) Frisch, Æ.; Frisch, M. J. *Gaussian 98 User's Reference*; Gaussian Inc.: Pittsburgh, PA, 1998.

(89) Benson, S. W. *Thermochemical Kinetics. Methods for the Estimation of Thermochemical Data and Rate Parameters*, 2nd ed.; John Wiley & Sons: New York, 1976.

(90) Reed, A. E.; Curtiss, L. A.; Weinhold, F. *Chem. Rev.* **1988**, *88*, 899−926.

(91) Gonzalez, C.; Schlegel, H. B. *J. Phys. Chem.* **1990**, *94*, 5523−5527.

(92) Wiest, O.; Black, K. A.; Houk, K. N. *J. Am. Chem. Soc.* **1994**, *116*, 10336−10337.

(93) Davidson, M. M.; Hillier, I. H. *Chem. Phys. Lett.* **1994**, *225*, 293−296.

(94) Davidson, M. M.; Hillier, I. H. *J. Chem. Soc., Perkin Trans. 2* **1994**, 1415−1417.

(95) Dewar, M. J. S.; Healy, E. F. *J. Am. Chem. Soc.* **1984**, *106*, 7127−31.

(96) Kupczyk-Subotkowska, L.; Saunders, W. H., Jr.; Shine, H. J.; Subotkowski, W. *J. Am. Chem. Soc.* **1993**, *115*, 5957−5961.

Table 3. Computed Energies, Zero-Point Energies, Enthalpies, Entropies, and Bond Distances with Bond Orders for Optimized Model Structures[a]

compound	E_{el}, hartree	ZPE [kcal/mol]	H [kcal/mol]	S [eu]	d(C–O) [Å] (BO)	d(C–C) [Å] (BO)	ΔH [kcal/mol]	ΔS [eu]	$\Delta\Delta H^{\ddagger}$ [kcal/mol]
1 GS	−425.362721	120.84	126.45	87	1.458 (0.86)	4.018 (0.002)	0	0	
1 TS	−425.321298	119.60	124.88	83.71	1.995 (0.366)	2.409 (0.299)	24.4	−3.29	−2.73
1 prod	−425.394506	121.13	126.74	87.43	3.961 (0.0006)	1.550 (0.976)	−19.7	0.43	
2 GS	−386.045983	102.52	107.47	81.96	1.456 (0.868)	4.079 (0)	0	0	
2 TS	−385.98664	100.86	105.64	80.32	2.176 (0.279)	2.594 (0.259)	35.4	−1.64	8.25
2 prod	−386.074181	102.71	107.65	82.17	3.921 (0)	1.548 (0.983)	−17.5	0.21	
6 global GS	−387.252149	116.02	121.98	90.09	1.442	4.667	0	0	
6 local GS	−387.24854	115.93	121.99	91.59	1.45	4.975	2.27	1.5	
6 chair TS	−387.200634	114.73	120.38	86.75	2.038	2.451	30.7	−3.34	3.57
6 boat TS	−387.198765	114.34	120.09	87.19	2.113	2.536	31.6	−2.9	4.45
7 global GS	−270.507198	74.69	79.57	80.96	1.403 (0.882)	5.28	0	0	
7 local GS	−270.504737	74.26	79.33	84.47	1.432 (0.891)	5.03 (0.0006)	1.31	3.51	
7 TS	−270.461159	73.50	77.83	75.66	1.904 (0.436)	2.314 (0.334)	27.16	−5.30	0
7 local prod	−270.533424	74.31	79.32	83.42	4.515 (0)	1.545 (0.99)	−16.70	2.46	
7 global prod	−270.533564	74.31	79.40	84.23	5.9	1.549 (0.988)	−16.72	3.27	
8 global GS	−349.143939	110.23	116.94	96.59	1.434 (0.876)	5.343	0	0	
8 local GS	−349.1413	109.74	116.66	100.3	1.437 (0.886)	5.124	1.38	3.71	
8 TS	−349.093446	108.51	114.78	90.2	2.401 (0.299)	2.001 (0.366)	29.53	−6.39	2.38
9 false global GS	−349.132045	109.67	116.25	92.97	1.459 (0.843)	5.601 (0)	4.37	−0.8	
9 linear GS	−349.135053	109.24	115.98	96.06	1.456 (0.855)	5.807 (0)	2.21	2.29	
9 local=globalGS	−349.13868	109.42	116.04	93.77	1.457 (0.853)	5.066	0	0	
9 TS	−349.099664	108.38	114.66	90.12	1.981 (0.371)	2.397 (0.293)	23.1	−3.65	−4.06
10 GS	−580.198444	167.11	173.59	92.7	1.475 (0.849)	3.199 (0.009)	0	0	
10 TS	−580.172855	165.47	171.83	91.73	1.965 (0.389)	2.389 (0.284)	14.3	−0.97	−12.9
10 prod	−580.240921	166.97	173.67	95.02	3.700 (0.0007)	1.562 (0.958)	−26.6	2.32	
11 local GS	−426.541881	134.04	140.67	94.31	1.469 (0.853)	3.088 (0.011)	0	0	
11 TS	−426.519978	132.70	139.05	91.9	1.946 (0.407)	2.360 (0.299)	12.13	−2.41	−15.0
11 local prod	−426.585943	133.57	140.55	99	4.382	1.553	−27.8	4.69	
12 GS	−582.587804	192.7	201.4	110.28	1.478 (0.842)	2.875 (0.024)	0	0	
12 TS	−582.571291	191.36	199.81	108.12	1.903 (0.435)	2.330 (0.294)	8.77	−2.16	−18.39
13 GS	−543.260256	175.13	182.97	103.08	1.487 (0.843)	2.744 (0.025)	0	0	
13 TS	−543.248995	173.67	181.37	102.18	1.812 (0.516)	2.265 (0.287)	5.47	−0.9	−21.69
14 GS	−776.734105				1.495 (0.833)	2.625 (0.040)	0		
14 TS	−776.725854				1.779 (0.546)	2.247 (0.280)	3.6		−23.6
15 GS	−308.594704	78.32	83.24	81.87	1.472 (0.869)	5.22	0	0	
15 TS	−308.536105	77.05	81.64	78.38	2.182 (0.32)	2.907 (0.207)	35.2	−3.49	8.02
15 prod	−308.659167						−40.5		

[a] E_{el}, the computed electronic energy in hartree/particle, 1 hartree = 627.51 kcal/mol; ZPE-zero point correction to E_{el}; H, thermal correction to enthalpy; d, distance in Å for breaking C–O and forming C–C bonds; BO, Wiberg bond order.

Table 4. Comparison of Results Obtained Using Various Levels of Theory for the Claisen Rearrangement of Allyl Vinyl Ether

method	$\Delta(E+ZPE)^{\ddagger}$ [kcal/mol]	$\Delta H^{\ddagger}$ [kcal/mol]	$\Delta S^{\ddagger}$ [eu]	d(C–O)‡ [Å]	d(C–C)‡ [Å]	ref
SVWN/6-31G*	20.8			1.696	2.094	93
BLYP/6-31G*	21.1			1.959	2.428	93
Becke3LYP/6-31G*	26.8			1.902	2.312	93
Becke3LYP/6-31G*	27.7	27.2	−5.3	1.904	2.314	this work
Becke3LYP/6+311G**	26.1			1.954	2.384	93
RHF/6-31G*	47.7			1.918	2.266	93
RHF/6-31G*	48.9[a]	46.9	−5.9 (298 K)	1.918	2.266	95
CASSCF/6-31G* (6e/6o)	42.5			2.100	2.564	93
MP2/6-31G*		24.3		1.799	2.202	94
MNDO		39.5	−13.4 (453 K)	1.46	1.88	96
			−12.8 (373 K)			
experiment, gas phase		29.42	−8.4 (458 K)			79
experiment, Bu$_2$O		25.4	−15.9 (373 K)			83
experiment, C$_6$D$_6$		25.72	−14.1			51

[a] $\Delta E_{el}^{\ddagger}$ only, not corrected with ZPE.

Analysis of computed molecular properties for the allyl vinyl ether local minimum and the corresponding transition state (Figure 6) suggests at least three potential sources of rate acceleration:

1. *Termini compression.* The reacting termini in the vinyl allyl ether local minimum are well-separated (5.03 Å) relative to the transition state (2.31 Å, Figure 6). Compression of the terminal olefinic carbons to a shorter contact distance, either by introducing a covalent skeleton or by confining the reactant to a limited volume within an enzyme active site, can be expected to induce a significant rate acceleration.

2. *Charge influence.* The NBO charge at oxygen varies insignificantly from reactant to TS (−0.45 to −0.46), as does the charge difference between the allyl and vinyloxy moieties (+0.26 vs +0.21). A delocalized aromatic transition state with a low sensitivity to polar effects is suggested. However, the molecular dipole moment exhibits a modest increase during rearrangement, as expected for a system undergoing conforma-
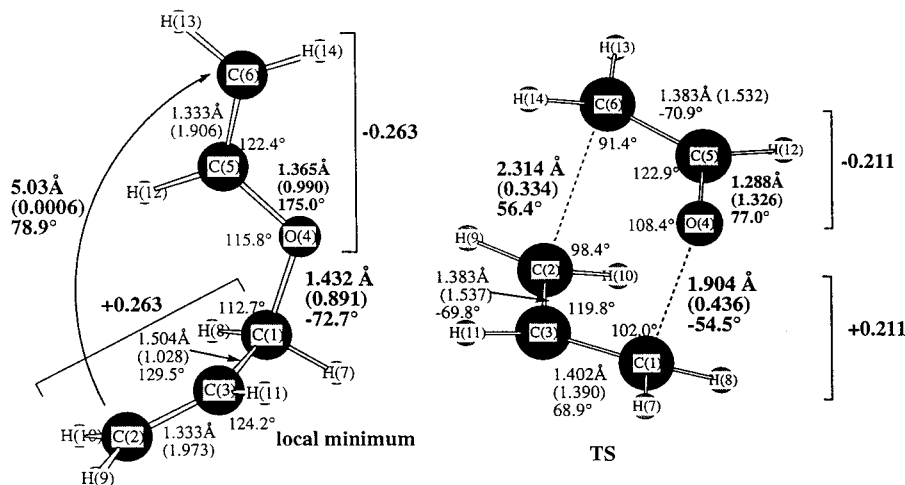
Figure 6. Analysis of molecular properties of the reactant (allyl vinyl ether **7**) and its Claisen chairlike transition state at the Becke3LYP/6-31G* level of theory. Values shown are bond distances, bond and torsion angles between heavy atoms, Wiberg bond orders (in parentheses), and group charges. Geometric parameters in bold correspond to key bonds being made and broken during the reaction. Signed numbers refer to the sum of calculated atomic charges for each three-atom fragment, the total molecular charge being zero. Numbering of atoms is arbitrary.

tional reorganization: reactant global minimum (0.92), local minimum (1.8), TS (2.1), and product (2.7 D) (**7**, Figure 4). Similar charge and dipole moment fluctuations were calculated for all other model systems (see Supporting Information for details). An increase in dipole moment at the transition state explains the experimentally observed small rate increase in polar solvents resulting from effective dipole–dipole interactions between transition state and the solvent. However, much stronger ion–dipole interactions might induce a larger stabilization of the Claisen transition state. This can be achieved, for example, by placing a cation near the substrate oxygen in the active site of chorismate mutase. In a model system, Wiest and Houk showed that the ammonium cation stabilizes the Claisen TS by 11.4 kcal relative to the reactant at the RHF/6-31G** level.[58] By contrast, neutral water gave only 2.6 kcal/mol stabilization at the same level of theory. Our Becke3LYP calculations also predict a 10–11 kcal/mol stabilization of the Claisen TS by NH_4^+ in the gas phase. However, counterions and solvation effects in real systems substantially diminish the catalytic effect of charged particles. The subject will be discussed in more detail in a separate paper.[66]

3. Complexation at oxygen. The Lewis acid-catalyzed Claisen rearrangement is a well-documented reaction.[53,54] The moderate rate acceleration of Claisen rearrangement in H-bonded solvents is also well-established, having been studied both experimentally and computationally.[1,58,59] Clearly, the relative energy of the transition state can be lowered by a catalyst that forms a full or partial bond with oxygen through its nonbonding electrons. Furthermore, the long C- - -O bonds in the transition state reduce steric demands at oxygen and assist interactions with potential complexing agents. Proton transfer is a particularly attractive mechanism in this respect. In one model calculation, protonated allyl vinyl ether was predicted to experience an activation barrier fall of 39.3 kcal/mol at the RHF level of theory.[58] Not surprisingly, the chorismate mutase enzyme likewise appears capable of stabilizing the Claisen TS by positioning H-bond donors (e.g., Lys or Arg) in the vicintiy of oxygen and the transforming C- - -O bond (Figure 1).

IRC Calculations for Allyl Vinyl Ether Rearrangement. Insights into the forces behind rate acceleration of the aliphatic Claisen rearrangement were obtained by analysis of the calculated minimum energy reaction pathway derived from individual IRC calculations as the optimized TS decays to reactant (allyl vinyl ether) and product (4-pentenal) (Figure 7). Chemical transformation, characterized by substantial changes in C–O and C–C bond distances and orders (Figure 8), occurs only during a short portion of the path near the transition state when the olefinic termini are compressed to a distance less than the sum of their van der Waals radii (3.4 Å[97]).

The first and the longest portion of the path is characterized by conformational reorganization around the three σ-bonds in allyl vinyl ether (RC from −20 to −12 amu$^{-1/2}$ × bohr and $d_{C1--C6} \geq 4.0$ Å; Figure 7). The corresponding energy increase is no more than 3 kcal/mol. Within the second, intermediate portion of the path, the calculated structures maintain nonstationary chairlike shapes with gradual compression of the reacting termini from 4.0 to 2.6 Å. While the energy rises by 15 kcal/mol, very little bond reorganization takes place. For example, at a distance of 3.06 Å between termini, the C1- - -C6 bond is 2% formed (RC = −4.8) based on bond order analysis. At 2.60 Å (RC = −2.1) near the end of this pathway segment, C1- - -C6 bond formation is estimated to be only 8% complete, while the C–O bond retains 89% of its single-bond character.

The third and shortest path segment of the route to the transition state, 2.6–2.3 Å, requires a final 10 kcal/mol and is characterized by substantial bond redistribution. At the TS barrier maximum ($d_{C1--C6} = 2.314$ Å, RC = 0, Figure 7) the C1–C6 and C–O bonds are present to the extent of 34 and 49% of their single-bond values, respectively. C1–C6 bond formation clearly compensates for both C–O bond scission and the van der Waals penalty associated with termini compression during rearrangement. Further progress along the reaction pathway rapidly culminates the exergonic bond exchange process and delivers the 1-hexenal product. Thus, at a reaction coordinate of +3.5 and $d_{C1--C6} = 1.709$ Å, C1- - -C6 bonding is 90% complete and accompanied by an energy drop of 25 kcal/mol.

The energy increase along the pathway is greatest for the second phase, during which molecular compression is resisted by van der Waals repulsions and unrelieved by C1–C6 bond formation. Were it possible to generate a stable or low-energy form of an intermediate along this path segment, an acceleration

(97) Bondi, A. van der Waals Volumes and Radii. *J. Phys. Chem.* **1964**, *68*, 441–451.
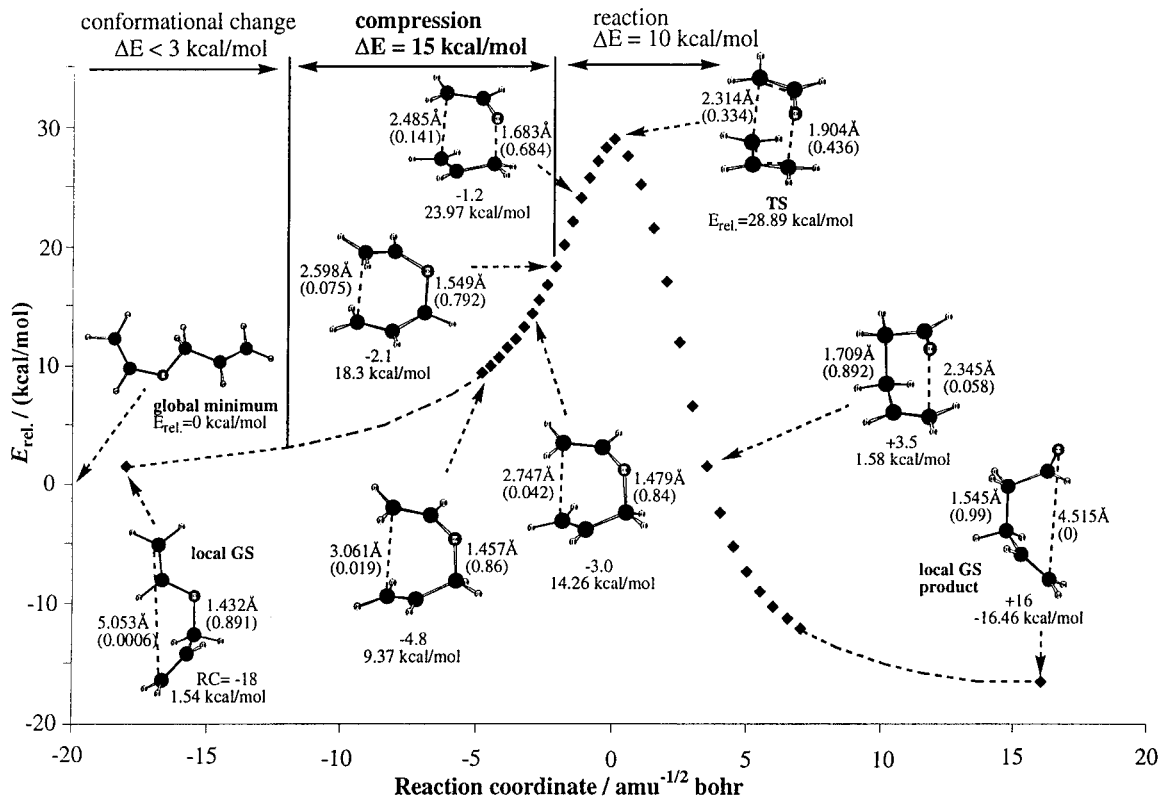
Figure 7. Minimum energy reaction pathway from allyl vinyl ether to 4-pentenal derived by individual intrinsic reaction coordinate (IRC) calculations.
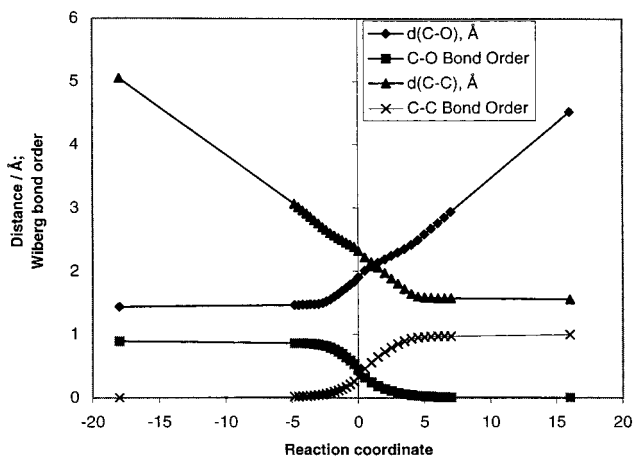

Figure 8. Change of distances and bond orders during rearrangement of allyl vinyl ether **7**.

of the rearrangement should result. Furthermore, the rate increase ought to be proportional to the degree of C1−C6 compression achieved in accord with the assumption of the spatiotemporal rule that the main component of the reaction coordinate on a multidimensional energy surface is the distance between reacting centers. Plots derived from the IRC calculations for allyl vinyl ether (Figure 8) are suggestive. They show a clear-cut relationship between the key bond distances and the mass-weighted reaction coordinate. The idea is applied to various model Claisen rearrangements described below.

Other Model Systems. The Becke3LYP/6-31G* protocol was applied to stationary points (i.e., GS and TS) on the reaction pathway for compounds **1**, **2**, and **6**. Calculated barriers ($\Delta H^{\ddagger}$ = 24.4, 35.4, and 30.7 kcal/mol, respectively) are in excellent agreement with the measured activation parameters ($\Delta G^{\ddagger}(C_6D_6)$ = 25.2, 34.9, and 31.2 kcal/mol, respectively; Table 2).

Chorismate itself (Scheme 1) rearranges without catalyst in aqueous solution at pH 7.5 with $\Delta H^{\ddagger}$ = 20.5 and $\Delta G^{\ddagger}$ = 24.2 kcal/mol (Table 1). Given that the pK_a's for carboxylic acids fall in the range of 2−3, both carboxylic centers are ionized under the reaction conditions. Accordingly, we have examined the concerted rearrangement for both the dianionic and neutral species. In the charged transition state, electrostatic repulsion results in a rather loose activated complex with d_{C-O} = 2.265 Å and d_{C-C} = 2.718 Å. The optimized distance between carboxylates is 5.34 Å. The neutral transition state, by contrast, displays shorter C- - -O and C- - -C bond lengths of 2.149 and 2.478 Å, respectively, and a 4.71 Å separation of carboxylates. Both factors allow the migrating 3,3 fragments to engage in tighter bonding. The corresponding Becke3LYP/6-31G* activation enthalpies are 43.1 and 26.6 kcal/mol for the dianionic and neutral processes, respectively. The latter value overestimates the measured $\Delta H^{\ddagger}$ by 6 kcal/mol, but is far superior to the charged estimate. We take this to mean that aqueous solvation strongly mitigates the electrostatic repulsion apparent in the modeled gas-phase dianionic pathway. Simple carboxylate protonation thus provides a sensible energetic approximation and probably also geometric representation of the charged, solvated aqueous system.

IRC calculations from both transition states resulted in different local minima. In the neutral case, the minimum nearest to the transition state is the chairlike pseudo-diaxial conformation. However, repulsion between carboxylates in the charged chorismate leads to the pseudo-diequatorial conformer with an intramolecular H-bond between ring hydroxyl and pyruvyl carboxylate. According to studies by Wiest and Houk, this conformer is a global conformational minimum.[58]

Finally, the activation barriers for eight other alkyl-substituted Claisen systems have been estimated by DFT methodology: **8**−**15** (Figures 4 and 5). While empirical values are not yet
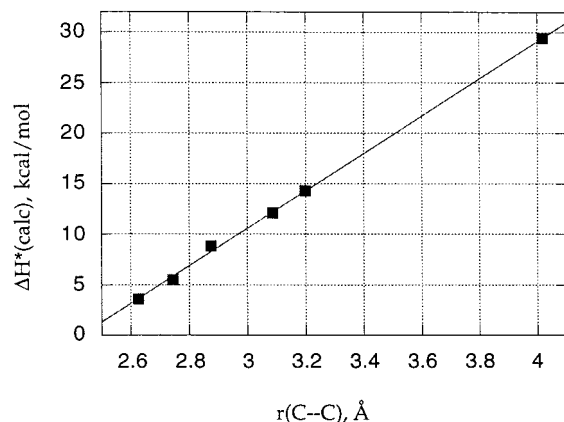
Figure 9. Plot of Becke3LYP/6-31G* activation barriers vs ground-state C- - -C termini separation for the Claisen rearrangement of structures **1** and **10−14** (Figure 5); $\Delta H^{\ddagger} = 18.513(r(\text{C- - -C})) - 44.95$, $r^{**}2 = 0.9995$.

known for these compounds, the predicted activation energies range from 35.2 to 3.6 kcal/mol (Table 3).

Spatiotemporal Theory versus Traditional Entropy Theory. The predicted behavior of compound **1** and structures **10−14** under Claisen conditions is a straightforward and unambiguous example of the operation of spatiotemperal theory. Figure 5 pictures the series and illustrates the regular drop in Becke3LYP/6-31G* activation enthalpy from 29.4 to 3.6 kcal/mol and the monotonic descent of ground-state C- - -C termini distances from 4.02 to 2.63 Å. The total drop in energy of $\Delta\Delta H^{\ddagger} = -25.8$ kcal/mol is accompanied by an overall compression of $\Delta r(\text{C- - -C}) = 1.39$ Å. A plot of these quantities is linear and characterized by an $r^{**}2 = 0.99$ (Figure 9). By contrast, the corresponding transition-state distances span a much smaller window ($\Delta r(\text{C- - -C}) = 0.16$ Å), while the NBO bond orders illustrate that C- - -C bond formation is similarly established for each of the structures in question (BO 0.28−0.30, Figure 5). The distance−energy relationship is clearly a ground-state effect. By incorporating allyl vinyl ether into a polycyclic architecture with decreasing spatial separation between the reactive centers, the rate of the rearrangement is projected to increase in a predictable and distance-dependent fashion using a single reaction coordinate.

The merits of the spatiotemporal principle and traditional entropy theory of enzyme and intramolecular catalysis have been the subject of a debate between Menger and groups such as those of Page, Jencks, and Houk.[61,63,72] Entropy theory provides an alternative explanation for extremely fast intramolecular and enzymatic reactions. It is based on two energy functions, enthalpy and entropy, which can be difficult to disentangle.[89] Entropy quantitatively describes the distribution of energy among all possible $3N$ degrees of freedom. For example, conversion of six translational and six external rotational degrees of freedom into three translational, three rotational, and six vibrational/internal rotational degrees of freedom when a bimolecular reaction is reconstituted as a unimolecular or an enzymatic reaction may contribute as much as 30−50 eu (9−15 kcal/mol at 298 K) to rate acceleration.[71,72] However, this is not the case in the unimolecular rearrangement of chorismate, where only a relatively small entropic destabilization of the reactant can be achieved by converting at least two internal rotations about exocyclic σ-bonds into two higher frequency vibrational motions. Since the activation entropy of the Claisen rearrangement will always be negative or near zero in a cyclic TS, the maximum contribution to ground-state destabilization

of Claisen substrates by conformational restriction would be 8−12 eu (maximum 3.6 kcal/mol). This conclusion is fortified by the recent work of Bruice and Lightstone in their analysis of lactonization rates for dicarboxylic acid monoesters.[98] By means of tandem quantum chemical and molecular dynamics calculations, they have provided further confirmation of the spatiotemporal principle while reaffirming that transition-state formation is under enthalpic control.

It is important to realize that spatiotemporal and entropic effects are not in conflict. This is not a matter of truth but, instead, a matter of which model is the more useful. We contend that entropy of reactions in solution are often beset with complexities (including those caused by solvent participation) that render the parameter difficult to interpret. In contrast, distance is a simple parameter that can often be measured or calculated precisely.

The predicted rearrangement rates for **1** and **10−14** can be understood in light of strain theory by noting that all the C- - -C termini distances and other atom−atom separations for **10−14** are less than the standard C−C van der Waals sum of 3.4 Å. The concomitant van der Waals repulsions incrementally raise the energy of the ground states and thereby reduce the energy gaps to the common transition state. In the absence of fully optimized ground- and transition-state structures at a common and reliable level of theory, however, quantitative estimates of strain energy and reaction barriers are a challenge. In the context that ground-state structure is the origin of variations in $\Delta H^{\ddagger}$ or $\Delta G^{\ddagger}$, distance is a simple, useful, and comprehensible parameter that can be either determined experimentally by X-ray crystallography or estimated by computational methods. And, as already derived mathematically,[63] the relationship between rate and distance is demonstrable from first principles. It applies to both small molecule reactivity and transformations mediated by enzymes. We know of no X-ray structure of an enzyme complexed with a good substrate analogue in which the crucial reactive groups are not placed at contact distances. *Rigid contacts are the common thread among all enzymes.* Thus, when used judiciously, the distance concept provides a convenient guide to prediction of relative reaction rates.

Selective Strain Attenuation at the Transition State. Not all transformations are neatly categorized by a simple application of either the spatiotemporal idea or ground-state strain analysis. Compare compounds **1** and **2**. The DFT optimized C- - -C distances differ by 0.06 Å (Figure 5). Spatiotemporal analysis suggests equally rapid rates of rearrangement. Similarly, the calculated exothermicities for the two reactions are comparable (-19.7 and -17.5 kcal/mol, respectively), leading to the same conclusion regarding strain energy considerations. Experimentally, it costs compound **2** an additional 9.7 kcal/mol relative to **1** to pass through its reorganization transition state in C_6D_6. The Becke3LYP/6-31G* estimate is 11.0 kcal/mol. A more extreme case is the modeled rearrangement of β-lactone **15**. The Claisen transition state requires an extra 10.8 kcal/mol relative to **1**. Since the four-membered ring to cyclohexenone transformation is predicted to be twice as exothermic as that for **1** (-40.5 kcal/mol, Table 3), ground-state strain release is clearly inoperative as a rate determinant. By contrast, $r(\text{C- - -C}) = 5.28$ Å in **15**. As the latter is 1.26 Å longer than in **1**, the significantly greater activation barrier superficially fulfills the spatiotemporal distance requirement, as it reflects the underlying energy requirements. Application of the equation used in Figure 9,

(98) Bruice, T. C.; Lightstone, F. C. *Acc. Chem. Res.* **1999**, *32*, 127−136.

however, predicts the rearrangement barrier for **15** to be 51.7 kcal/mol, 16.5 kcal/mol higher than the optimized DFT transition state.

Structures **2** and **15** with large rearrangment barriers of 35.4 and 35.2 kcal/mol (Table 3), respectively, share some critical common features. In particular, the three-atom enolate and allylic fragments participating in the sigmatropic shift transition states experience considerably less bonding than in **1**. This is evidenced primarily by the considerably shorter bond lengths in the latter: for **1**, **2**, and **15**, $r(C{-}{-}C) = 2.409, 2.594, 2.907$ Å and $r(C{-}{-}O) = 1.995, 2.076, 2.182$ Å, respectively. Bond strength as measured by covalent bond order decreases in the same order: $BO(C{-}{-}C) = 0.30, 0.26, 0.21$ and $BO(C{-}{-}O) = 0.37, 0.28, 0.32$, respectively. In an attempt to achieve maximal bonding between both ends of the shifting three-atom units, each partially formed bond suffers in response to an exceptional strain increase required to move from ground state to transition state where orbital overlap is relatively poor; bonds are stretched and binding capacity is sacrificed. The favorable phase 2 compression described above for vinyl allyl ether (Figure 7) is obstructed in **2** and **15** by geometric forces. The induction of transition-state strain along the reaction pathway is unanticipated by ground-state geometry or energetics.

A less dramatic illustration of the same point is given by compounds **3**–**6**, which rearrange with additional energy requirements of 6.0–8.4 kcal/mol relative to **1**. The systems likewise experience transition-state strain not present in the olefinic ground states. As described in the section on Kinetic Measurements, the axial chair conformation necessary for achieving a concerted Claisen transition state is destabilized by 1,3-diaxial interactions in all these cases. The Becke3LYP/6-31G* method accurately mirrors the differential TS/GS strain effects as probed with structure **6**. One unusual and unexplained result is the observation that **5** and **6** rearrange cleanly with nearly identical energy requirements in benzene-d_6 (Table 2), although **5** is anchored by a *tert*-butyl group. Since the enthalpic energy requirements for rearranging by means of a chair or a boat transition state for **6** differ by only 0.9 kcal/mol (Table 3), we surmise that **5** is able to place the bulky t-Bu group in a flattened axial position of the cyclohexene ring and transform to product through the boat transition state (cf. Figure 4).

In cases such as **2**–**6** and **15**, neither spatiotemporal nor classical strain energy considerations carry the capacity to predict relative rates of reaction. Each approach could be parametrized to handle the Claisen rearrangement and other reactions, of course, but then the simplicity of the schemes is lost.

The situation is not novel. Some years ago a correlation was observed between both ground-state strain energies and acetylenic C$\cdot\cdot\cdot$C bond distances as derived from force field calculations and the rates of cycloaromatization for a limited set of enediynes synthesized as esperamicin and calicheamicin mimics. A spatiotemporal rule of thumb was proposed that spontaneous cyclization at room temperature will occur for a C$\cdot\cdot\cdot$C bond distance in the range of 3.31–3.20 Å.[99] Exceptions to the generalization were revealed simultaneously. Both experiment[100,101] and theory[102,103] and their combination[104] demonstrated that while certain enediynes enjoy strain release early

on the path to the transition state leading to the 1,4-diyl biradical, the cyclization rates of many others are governed by strain attenuation manifested only at the activated complex along the same path. Subsequently, similar observations were made for the dynemicin enediyne family.[105–107]

What the current and previous studies teach is that relative rate estimates based on ground-state or intermediate[108] properties alone can be a misleading exercise. For the Claisen rearrangement and cycloaromatization of enediynes, a subset of structures (e.g., **1**, **10**–**14**) obeys a proximity rule based on ground-state geometry. However, for these two reactions and any other class subjected to a similar analysis, a broader representation of structures will always reveal many outliers. Since reaction rates mirror *energy differences* between two states (ground and transition), cases can always be found or designed in which differential strain energy between the two stationary points sabotages an ambitious generalization based on only one of them. Where it is suspected that rate data do not behave cleanly as illustrated in Figure 9, the most judicious approach is explicit modeling of both ground and transition states by a suitable quantum chemical procedure.

Rationalization of Chorismate Mutase and Antibody Catalysis from the Model Studies. We tentatively conclude that chorismate mutase achieves its catalysis by a combination of three effects.

(1) The enzyme captures the pseudo-diaxial conformer of the substrate in a loose prereactive chairlike geometry. The contribution of such a conformational selection to catalysis is not particularly significant (<3 kcal/mol). It is, however, consistent with the smaller catalytic effect observed for the two catalytic antibodies relative to that for chorismate mutase.

(2) Protein compression of the reactive termini destabilizes the ground state with a concomitant large drop in $\Delta G^{\ddagger}$. The situation is pictured in the compression phase of Figure 7. Only a modest amount of energy need be expended by the enzyme to orient the substrate for passage through the activated complex without entering the final bond-making and bond-breaking phase of the pathway. We believe that chorismate mutases achieve the effect in part by lining the binding pocket with hydrophobic residues that anchor the substrate by means of short van der Waals forces. For example, the enzyme from *B. subtilis* presents Phe54 and Leu115 on opposite sides of chorismate and appears to pin the reactive termini into an orientation that anticipates subsequent rearrangement (Figure 10). Val35 may play a similar role in the *E. coli* enzyme. Evolutionary pressure could have intervened to incorporate such space-occupying amino acids and thus improve the enzymes' catalytic capacity.

Compaction of chorismate at the active site is compensated by multiple ionic and polar interactions, presumably the main contributors to the binding energy. While ionic interactions in the interior of a protein are generally weakened as part of a web of competing interactions between counterions, water, and polar groups,[109] chelation of pyruvyl carboxylate with Arg7, Arg90, and Tyr108 (Figure 10) nonetheless represents a potent mechanism for carboxylate identification and restriction. Hy-

(99) Nicolaou, K. C.; Zuccarello, G.; Ogawa, Y.; Schweiger, E. J.; Kumazawa, T. *J. Am. Chem. Soc.* **1988**, *110*, 4866–4868.

(100) Magnus, P.; Carter, P. A. *J. Am. Chem. Soc.* **1988**, *110*, 1626–1628.

(101) Magnus, P.; Lewis, R. T.; Huffman, J. C. *J. Am. Chem. Soc.* **1988**, *110*, 6921–6923.

(102) Snyder, J. P. *J. Am. Chem. Soc.* **1989**, *111*, 7630–7632.

(103) Snyder, J. P. *J. Am. Chem. Soc.* **1990**, *112*, 5367–5369.

(104) Magnus, P.; Fortt, S.; Pitterna, T.; Snyder, J. P. *J. Am. Chem. Soc.* **1990**, *112*, 4986–4987.

(105) Snyder, J. P.; Tipsword, G. E. *J. Am. Chem. Soc.* **1990**, *112*, 4040–4042.

(106) Magnus, P.; Carter, P.; Elliott, J.; Lewis, R.; Harling, J.; Pitterna, T.; Bauta, W. E.; Fortt, S. M. *J. Am. Chem. Soc.* **1992**, *114*, 2544.

(107) Magnus, P.; Fairhurst, R. A. *J. Chem. Soc., Chem. Commun.* **1994**, 1541–1542.

(108) For example, the putative local minima termed NACs (near attack conformations) by Bruice and Lightstone; ref 98.

(109) Scheiner, S.; Kar, T. *J. Am. Chem. Soc.* **1995**, *117*, 6970–6975.
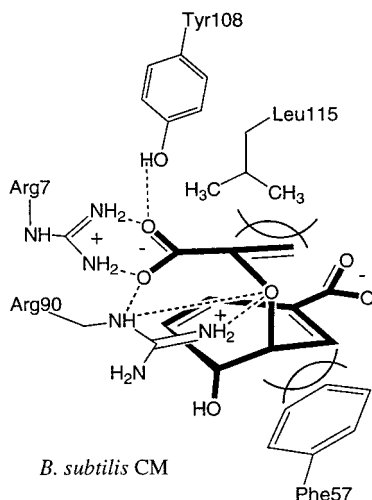
Figure 10. Conformational restriction and compression of the enol-pyruvyl moiety of chorismate at the active site of the *B. subtilis* chorismate mutase (only selected residues are shown).[9]

drophilic and hydrophobic residues thus conspire to position and prepare the substrate for bond reorganization.

Chorismate bound to an abzyme from antibodies may experience a qualitatively different environment. Formed over a short time period, antibodies generally recognize polar functionalities. Immobilizing interactions between abzymes and a nonpolar substrate moiety represent a weak and improbable source of specific recognition. Consequently, in the absence of a balanced combination of steric and electrostatic forces, the enolpyruvyl side chain of chorismate in an abzyme most likely experiences varying degrees of rotational mobility. *Even modest motional freedom would be highly deleterious to the rearrangement rate*. A variable degree of catalytic efficiencies is the conceivable outcome. In agreement, the weakly catalytic antibody 1F7 exhibits no short van der Waals contacts at the active site and many fewer polar ones relative to chorismate mutases (Figure 2). In particular, as described by Hilvert et al.,[14] short-range ionic interactions with carboxylates are completely missing in 1F7. As a result, not only does the abzyme lack an efficient steric compression mechanism but also the relatively sparse electrostatic machinery would appear to be able to offer only a limited compensation for whatever compression is in fact achieved.

The increasing repulsive interaction of the two carboxylates in chorismate engendered during compression is relieved by the neutralizing effect of two positively charged arginines (Figure 1). According to computational studies by Wiest and Houk,[58] the stabilization of such repulsive interactions contributes nearly 6 kcal/mol to catalysis. Unfortunately, there is no simple experimental way to ascertain the distance between reactive termini in chorismate while complexed with the enzyme. However, combined quantum and molecular mechanical modeling (QM/MM) of the *B. subtilis* enzyme by Mulholland et al.[56] gave 2.849 Å for this distance as compared to 3.298 Å for chorismate in the gas phase. Let us assume that the enthalpy–distance regression equation obtained for internally constrained vinyl allyl ether analogues (Figure 9) applies to these quantities, the first of which arises from external constraint of the same functionality. The estimated activation enthalpies of 7.8 and 16.1 kcal/mol fall below and near measured enzyme rearrangement barriers, respectively (Table 1). The compressed complex clearly enjoys a substantial advantage. In light of this comparison and that illustrated by **1** and **10**−**14** (Figure 9), we estimate that

steric compression at the enzyme active site has the potential to contribute ≥ 10 kcal/mol to barrier lowering.

In a second QM/MM study, Hillier and colleagues demonstrated that interactions between active site and ligand are maximal for structures close to the TS geometry and that they lead to a barrier lowering greater than that needed to produce the observed rate accelerations.[57] Conformational restriction, worth many orders of magnitude in rate, would appear to provide the major contribution to catalysis. It is associated with a large decrease in activation enthalpy in addition to a minor reduction in $T\Delta S$ arising from entropy loss during compression of the ground state.

(3) At this time, we cannot exclude the possibility that selective elecrostatic transition-state stabilization provides an important contribution to chorismate mutase catalysis. However, separate studies[58,66] suggest that a strong ionic hydrogen bond to the ether oxygen of the Claisen reactant has a negligible catalytic effect relative to background reaction in aqueous media. Such H-bonding may nevertheless play a role in nonpolar media and in the gas phase.

The total catalytic effect summarized here is larger than that needed to explain the observed 3×10^6-fold catalysis by chorismate mutases (i.e., $\Delta\Delta G^{\ddagger} = 8$−$9$ kcal/mol, Table 1). We conclude that the rearrangement itself is not the rate-determining step, in agreement with experimental data and computational studies in the literature. The major contribution to catalysis could, in principle, come from the geometric disposition of chorismate at the active site via confinement of the reactive termini to short contact distances, a conclusion in harmony with and predicted by the spatiotemporal principle as it applies to a well-behaved series such as **1** and **10**−**14** (Figure 9).

Experimental Section

General Details. Melting points were determined with a Thomas-Hoover capillary melting point apparatus. Proton nuclear magnetic resonance spectra (^{1}H NMR) were obtained either on a General Electric QE-300 MHz FT high-resolution spectrometer or on a General Electric GN-500 MHz FT high-resolution spectrometer. High-resolution electron impact (EI), fast atom bombardment (FAB), and liquid secondary ion mass spectrometry (LSIMS) were recorded on a VG Analytical Instruments model VG-70S or JEOL at Emory University Mass Spectrometry Center. We acknowledge the use of Shared Instrumentation provided by grants from the NIH and the NSF. Elemental analyses were performed by Atlantic Microlab, Inc., P.O. Box 2288, Norcross, GA 30091. Infrared spectra (IR) were recorded on a Perkin-Elmer 983 infrared spectrometer. All silica gel used was EM Science 230−400 mesh silica gel (particle size 0.040−0.063 mm). Thin-layer chromatography (TLC) plates were obtained from Aldrich Chemical Co. as precoated silica gel sheets (thickness of 0.250 mm, 254 nm fluorescent indicator). TLC plates were observed with a UV light (254 nm). All starting materials and reagents were purchased from Aldrich Chemical Co. or noted otherwise. Solvents were purified as necessary where noted. Solvents used for the NMR were CDCl$_3$, 99.8 atom % D, purchased from Cambridge Isotope Laboratories (CIL), D$_2$O, 99.9% D (CIL), DMSO-d_6, 99.9 atom % D (Sigma), and benzene-d_6, 99.6% D (Aldrich).

Computational Methods. Quantum chemical calculations were performed with Gaussian 98W[86] on a Pentium II with dual 400 MHz CPU and 512 MB RAM or with Gaussian 94[85] on IBM RS6000 workstations at the Emerson Center for Scientific Computations at Emory University, Department of Chemistry. Force field calculations were carried out with either Chem3D Pro[110] or MacroModel.[87] All density functional theory calculations were performed at the Becke3LYP/6-31G* level of theory with a 50194 integral grid. Initial guesses of the transition-state geometries were obtained by constrained force field minimization with Chem3D. Optimization of transition-state geometries was performed using the standard frequency method or the STQN

method with the opt=(TS, QST3) keyword for large molecular systems such as **12**−**14**. Both methods gave identical results for system **11**. Initial geometries of reactants and products adjacent to the optimized transition states were located by constrained MM2 minimization of the transition-state structure or the last point of IRC calculations. The global conformational minima of reactants were derived from a Monte Carlo full conformational search in MacroModel with the MM3* force field, followed by optimization with Gaussian. All optimized structures were characterized by harmonic frequency analysis except **14**. All transition states were characterized by a single imaginary frequency ($N_{imag} = 1$). All reported thermochemical properties are calculated at 298 K. The bond orders are computed according to the Wiberg method implemented in the NPA/NBO facility of Gaussian.[90] IRC calculations were performed with mass-weighted Cartesian coordinates. The detailed results of calculations including Cartesian coordinates, 3D geometries with distances, bond and torsional angles, bond orders, charges, frequencies, and thermochemical properties have been placed in the Supporting Information and are available from the authors upon request.

Kinetics. Kinetic experiments for all compounds were performed in benzene-d_6 and in some cases in CDCl$_3$, DMSO-d_6, or D$_2$O. The kinetics was followed by reactant disappearance relative to a standard solvent signal or relative to the sum of integral intensities of reactant and product at the olefinic protons by means of proton NMR. NMR tubes were washed with 10% HCl, then with 10% NaOH for 1 h, then washed with water many times, and dried in an oven. Depending on the temperature (above or below the boiling point of solvent), regular or high-pressure/vacuum NMR tubes were used. In the case of regular NMR tubes, solutions were flushed with argon and sealed with a standard plastic cap. Solutions in pressure/vacuum NMR tubes were degassed by at least three freeze−pump−thaw cycles and sealed in a vacuum. NMR tubes with a solution of compound were placed into a thermostated bath (either a water bath with $\Delta T = \pm 0.1$°C for kinetic runs below 100 °C or an oil bath with $\Delta T = \pm 0.5$ °C, for kinetic runs above 100 °C). After measured time intervals the tube was periodically removed and quenched with ice, and NMR spectra were taken. Spectra were taken before the reaction and at least two times up to 50% reaction completion and finally at the end of reaction (>95% completion). For accurate measurements the time intervals should be at least 20 min assuming that approximately 1 min is required for temperature equilibration to reach bath temperature. In some cases, we used solutions sealed in melting point capillary tubes instead of solutions in a pressure NMR tube. The rate constants obtained by both methods were identical; however the capillary method was dangerous and often led to explosion due to bad sealing. Rate constants were obtained from first-order kinetic curves. The free energy of activation ($\Delta G^{\ddagger}$) was subsequently calculated at each temperature from the Eyring equation. Activation enthalpies ($\Delta H^{\ddagger}$) and entropies ($\Delta S^{\ddagger}$) were obtained from linear plots of $\Delta G^{\ddagger}$ versus T and calculated from Arrhenius parameters.[89] Results from the two methods including statistical analysis were identical. Statistical data analyses were performed with the Microsoft Excel program. Reported deviations correspond to the 95% probability limit.

3-Methylene-2-oxabicyclo[3.3.1]non-7-ene (**1**). The compound was prepared by a modified general procedure for Tebbe olefination of esters.[75] **Caution:** The Tebbe reagent, especially in the solid form, is extremely flammable and reacts violently with water. All operations must be done under inert atmosphere. All glassware was washed with HCl and water, then kept in 10% NaOH for 1 h, washed many times with water, and dried in an oven at 90 °C. A 50 mL three-necked round-bottom flask fitted with two rubber septums and vacuum inlet was heat-vacuum-dried at 200−300 °C, then filled with Ar, and cooled to ambient temperature. Pentane (25 mL) was added followed by Tebbe reagent (3 mL of 0.5 M Tebbe reagent in toluene, Aldrich) with stirring. The resulting brown precipitate was carefully decanted with a syringe. Addition of pentane and decantation were repeated twice more. Traces of solvent were removed under vacuum to constant weight, giving 781 mg of Tebbe reagent as brown flakes (2.74 mmol). THF (6 mL, anhydrous, Aldrich) was added, and the solution was cooled in a dry ice/acetone bath. Excess ester **16**[73,74] (748 mg, 2 equiv) was dissolved in THF (6 mL, anhydrous) with a small amount of anhydrous Na$_2$CO$_3$ and introduced via syringe into the reaction flask during ca. 1 min while

shaking. The cold bath was removed, and the resulting dark red solution was allowed to warm to ambient temperature for 5 min. After an additional 25 min the reaction was quenched with 0.5% triethylamine in pentane (20 mL) and cooled to 0 °C, and then 10% NaOH (2 mL) was added slowly with stirring. After 30 min, the water layer was frozen on a cold bath and extracted many times with 0.5% triethylamine in pentane. The combined organic solution was quickly filtered and eluted with 0.5% triethylamine at −78 °C via a 1 × 5 cm plug of basic alumina prewashed with the eluent in a funnel for cold filtration. Collected solution (50 mL) was evaporated at 20 °C. The residue was treated three times with 0.5% triethylamine in pentane followed by solvent evaporation to remove residual THF. Brown oil (400 mg) remained. Kugelrohr distillation at 40 °C gave 80 mg of colorless oil, containing ca. 15 mol % of triethylamine as stabilizer. Yield: 20%. The residue after distillation contained crude starting ester. To obtain pure product, Me$_3$N can be used instead of Et$_3$N.

Notes: When excess Tebbe reagent was used, it served as a Lewis catalyst for Claisen rearrangement of the desired product, leading to ketone **17** (bicyclo[3.3.1]non-6-en-3-one). This intermediate then reacted with the Tebbe reagent much faster than the starting ester to give 3-methylenebicyclo[3.3.1]non-6-ene as the only product. The product **1** is unstable under acidic conditions and isomerizes rapidly to the more stable exo-isomer **19** followed by ether cleavage in the presence of traces of water. In numerous unsuccessful attempts the exo-isomer was the only product. Double-bond migration took place when silica was used for separation, in commercial CDCl$_3$ which was not specially treated to remove traces of HCl, and even on basic alumina at ambient temperature. The desired product was obtained only by use of acid-free glassware and cold filtration over basic alumina prewashed with 0.5% Et$_3$N or Me$_3$N in pentane. ^{1}H NMR (300 MHz, C$_6$D$_6$, C$_6$D$_5$H = 7.16 d): δ = 5.68 (unres m, 2H; CH=CH), 4.58 (d, ^2J = 2.2 Hz, 1H; CH$_2$=), 4.25 (broad s, 1H; CH−O), 4.21 (dd, ^2J = 2.2 Hz, 2H; CH$_2$=), 2.30 (m, 1H), 1.60−1.95 (m, 5H), 1.35 (m, 2H). ^{1}H NMR (300 MHz, acid free CDCl$_3$, CHCl$_3$ = 7.26 d): 5.99 (m, 1H; CH=), 5.77 (m, 1H; CH=), 4.44 (broad s, 1H; CH−O), 4.23 (d, ^2J = 2.2 Hz, 1H; CH$_2$=), 4.14 (d, ^2J = 2.2 Hz, 1H; CH$_2$=), 1.6−2.6 (m, 7H). MS (high res EI): m/z: calcd for C$_9$H$_{12}$O 136.0888, found 136.0881.

Bicyclo[3.3.1]non-6-en-3-one (**17**). After completion of reaction, the solutions from selected Claisen rearrangement kinetic runs for **1** in C$_6$D$_6$ were combined and evaporated. The proton NMR and IR spectra were in aggrement with the literature data.[111,112] ^{1}H NMR (300 MHz, CDCl$_3$, CHCl$_3$ = 7.26 δ): δ = 5.72 (unres dm, $^3J_{cis}$ = ca. 10 Hz, 1H; - -CH=), 5.61 (ddd, $^3J_{cis}$ = 10.8 Hz, 1H; CH=), 2.69 (br s, 1H), 2.25−2.56 (m, 6H), 1.90−2.02 (m, 3H). IR (neat): 3025, 2923, 2865, 1715. MS (high res EI): m/z calcd for C$_9$H$_{12}$O 136.0888, found 136.0884.

7-Methylene-6-oxabicyclo[3.2.1]oct-3-ene (**2**). The compound was obtained by the same procedure as used for **1** starting from corresponding lactone **21**[113] with modifications: Reaction time was 1 h. The pentane solution of crude product obtained after cold filtration was evaporated at atmospheric pressure rather than by rotovap, since the product appears to be very volatile. THF was removed by quenching with pentane and evaporated at atmospheric pressure three times. A 300 mg sample of starting ester and 1 equiv of Tebbe reagent gave 40 mg of colorless oil after final Kugelrohr distillation at ambient temperature (13% yield). ^{1}H NMR (300 MHz, C$_6$D$_6$, C$_6$D$_5$H = 7.16 δ): δ = 5.81 (unres dm, 1H), 5.41 (unres dm, $^3J_{cis}$ = ca. 9.5 Hz, 1H), 4.54 (s, 1H; CH$_2$=C−O), 4.20 (t, ^3J = 5.2 Hz, 1H; CH−OR), 3.97 (s, 1H; CH$_2$=C−O), 2.60 (br s, 1H), 2.03 (dq, A part of AB(XYZ), ^2J = 18 Hz, ^3J = ^4J = 3 Hz, J_3 = 0 Hz, 1H; vinyl−CH$_2$), 2.03 (dm, B part of AB(XYZ), ^2J = 18 Hz, 1H; vinyl−CH$_2$), 1.76 (dt, ^2J = 10.5 Hz, ^3J = ^3J = 5.2 Hz, 1H; CH$_2$ axial), 1.43 (d, ^2J = 10.5 Hz, ^3J = ^3J = 0 Hz, 1H, CH$_2$ equatorial). ^{13}C NMR + APT (75 MHz, C$_6$D$_6$, C$_6$D$_6$ =

(110) *Chem3D Pro for Windows 95/NT*; CambridgeSoft Corporation: Cambridge, MA, 1997.

(111) Subramaniam, R.; Fort, R. C., Jr. *J. Org. Chem.* **1984**, *49*, 2891−2896.

(112) Henkel, J. G.; Hane, J. T. *J. Org. Chem.* **1983**, *48*, 3858−3859.

(113) Kuwahara, S.; Mori, K. *Tetrahedron* **1990**, *46*, 8075−8082.

128.39 δ): δ = 168.11 (=C(R)−O), 130.55 (down, one of CH=CH), 129.88 (down, one of CH=CH), 80.95 (up, CH$_2$=), 73.70 (down, CH−O), 39.02 (down, CH), 35.67 and 35.54 (up, two CH$_2$). MS (high res EI) m/z calcd for C$_8$H$_{10}$O 122.0732, found 122.0744.

trans-5-tert-Butylcyclohex-2-enyl Vinyl Ether (3). The compound was synthesized according to a modified general procedure of Watanabe and Conlon.[114] Mercury(II) acetate was recrystallized from ethanol and dried in a vacuum immediately before use. Ethyl vinyl ether was washed with 1 M HCl and 10% NaOH, dried over Na$_2$CO$_3$, and stored over sodium before use. It was distilled directly into the reaction flask (20 mL) containing *trans*-5-tert-butylcyclohex-2-enol (**23**)[77] (300 mg, 1.95 mmol) under argon. Hg(OAc)$_2$ (60 mg) was added and refluxed under Ar for 4 h, then an additional 30 mg of Hg(OAc)$_2$ was introduced, and reflux was continued for another 6 h. The reaction mixture was cooled on an ice bath, stirred with 10% Na$_2$CO$_3$ (20 mL) for 10 min, and diluted with ether, and the layers were separated. The ether solution was dried (Na$_2$CO$_3$) and evaporated at room temperature to give 416 mg of a colorless liquid containing ca. 10% of unreacted alcohol by ^{1}H NMR. The crude product was dissolved in 0.4% Et$_3$N in pentane and quickly chromatographed at −78 °C on basic alumina prewashed with eluent. Evaporation gave 346 mg of product stabilized with Et$_3$N. ^{1}H NMR (300 MHz, concentrated in CDCl$_3$, CHCl$_3$ = 7.26 δ): δ = 6.35 (dd, $^3J_{cis}$ = 6.6 Hz, $^3J_{trans}$ = 14.1 Hz, 1H), 6.03 (ddd, $^3J_{cis}$ = 9.9 Hz, J = 5.4, 2.1 Hz, 1H), 5.82 (m, 1H), 4.32 (br s, 1H), 4.31 (dd, ^2J = 1.5 Hz, $^3J_{trans}$ = 14.1 Hz, 1H), 4.01 (dd, ^2J = 1.5 Hz, $^3J_{cis}$ = 6.6 Hz, 1H), 2.14 (m, 1H), 2.07 (m, 1H), 1.74 (m, 1H), 1.55 (t of dd, 1H), 1.25 (t of d, 1H), 0.87 (s, 9H). [13]C + APT (75 MHz, CDCl$_3$, CDCl$_3$ = 77.00 δ) δ = 150.53 (down, O−CH=), 133.80 (down, CH=), 124.21 (down, CH=), 88.24 (up, CH$_2$=), 71.93 (down, CH−OR), 37.84 (down, CH−t-Bu), 31.75 (up, C of t-Bu), 29.03 (up, CH$_2$), 27.08 (down, Me of t-Bu), 26.91 (up, CH$_2$). IR (neat): 3120, 3050, 2980, 2940, 2880, 1650, 1625, 1490, 1460, 1415, 1390, 1355, 1335, 1220, 1200, 1095. MS (high res EI): m/z calcd for C$_{12}$H$_{20}$O 180.1514, found 180.1519.

(trans-5-tert-Butylcyclohex-2-enyl)acetaldehyde (27). *trans*-5-tert-Butylcyclohex-2-enyl vinyl ether (**3**) in C$_6$D$_6$ was sealed in a capillary tube and kept at 150 °C for 3 days. The reaction mixture was dissolved in CDCl$_3$ for NMR and then evaporated in air for IR and MS analysis. NMR and IR spectra were in agreement with the literature.[115] ^{1}H NMR (300 MHz, 4:1 CDCl$_3$/C$_6$D$_6$, CHCl$_3$ = 7.26 δ): δ = 9.88 (t, ^3J = 2.0 Hz, 1H; CHO), 5.90 (unres m, 1H), 5.80 (unres m, 1H), 2.95 (m, 1H), 1.00−3.00 (20H). IR (neat): 1725. MS (high res EI): m/z calcd for C$_{12}$H$_{20}$O 180.1514, found 180.1508.

trans-5-tert-Butylcyclohex-2-enyl Acetate (28). *trans*-5-tert-Butylcyclohex-2-enol (**23**) (461 mg, 2.99 mmol) in anhydrous pyridine (5 mL, Aldrich) and acetic anhydride (5 mL, excess) was stirred overnight at room temperature (after 1.5 h reaction had reached only 40% completion), then poured into saturated NaHCO$_3$ with ice, stirred for 1 h, extracted with ether, washed with saturated NaHCO$_3$ twice, dried (Na$_2$SO$_4$), and evaporated to give 534 mg of pale yellow oil, yield 91%. Acetylation under acidic conditions (catalytic amount of H$_2$SO$_4$) led to a mixture of *cis*- and *trans*-isomers. ^{1}H NMR (300 MHz, concentrated in CDCl$_3$, CHCl$_3$ = 7.26 δ): 6.02 (ddd, $^3J_{cis}$ = 9.9 Hz, ^3J = 5.7 Hz, ^4J = 2.1 Hz, 1H), 5.75 (m, 1H), 5.26 (unres m, 1H), 1.99 (s, 3H), 1.22−2.13 (m, 5H), 0.83 (s, 9H). [13]C + APT (75 MHz, CDCl$_3$ = 77.00 δ): 170.52 (up, −CO$_2$Me), 134.15 (down, CH=), 123.78 (down, CH=), 67.71 (down, CH−O), 38.30 (down, CH), 31.65 (up, C of tBu), 29.45 (up, CH$_2$), 26.98 (down, CH$_3$), 26.72 (up, CH$_2$), 21.27 (down, CH).

trans-5-tert-Butylcyclohex-2-enyl 1-Methylvinyl Ether (4). *trans*-5-tert-Butylcyclohex-2-enyl acetate (**28**) (400 mg, 2.04 mmol) in 3 mL of anhydrous THF was mixed with Tebbe reagent (5 mL, 0.5 M in toluene, Aldrich) at −78 °C under argon atmosphere. The cold bath was removed and kept at room temperature for 30 min. Workup followed that for **1**. Kugelrohr distillation from Na$_2$CO$_3$ gave 214 mg of pale yellow oil. ^{1}H NMR (300 MHz, CDCl$_3$, CHCl$_3$ = 7.26 ppm): 6.04 (ddd, ^4J = 1.8 Hz, ^3J = 5.4 Hz, $^3J_{cis}$ = 9.6 Hz, 1H; ring CH=), 5.84 (m, 1H; ring CH=), 4.52 (br s, 1H; CH−O), 3.91 (s, 2H, CH$_2$=),

2.14 (m, 2H), 1.80 (s, 3H), 1.76 (m, 1H), 1.55 (m, 1H), 1.20 (t of d, J = 3.9, 13.2 Hz, 1H), 0.87 (s, 9H). [13]C + APT (75 MHz, C$_6$D$_6$, C$_6$D$_6$=128.07 δ): δ = 158.86 (up, small, O−C=), 133.19 (down, CH=), 125.53 (down, CH=), 82.08 (up, CH$_2$=), 69.57 (down, CH−O), 39.12 (down, CH), 32.13 (up, small), 29.40 (up), 27.78 (up, small), 27.62 (down, CH$_3$ of tBu), 22.50 (down). IR (neat): 3130, 3033, 2960, 2920, 2890, 2870, 2840, 1660, 1600, 1490, 1480, 1455, 1447, 1440, 1405, 1390, 1380, 1290. MS (high res EI): m/z calcd for C$_{13}$H$_{22}$O 194.1671, found 194.1663; m/z 138 C$_9$H$_{14}$O$^+$, 137 C$_{10}$H$_{17}^+$, 136 C$_{10}$H$_{16}^+$, 121 C$_9$H$_{13}^+$.

(trans-5-tert-Butyl-cyclohex-2-enyl)acetone (29). *trans*-5-tert-Butylcyclohex-2-enyl 1-methylvinyl ether (**4**) in C$_6$D$_6$ was sealed in a pressure/vacuum NMR tube after a few freeze−pump−thaw cycles and kept in an oil bath at 150 °C for 3 days. ^{1}H NMR (400 MHz, benzene-d_6, C$_6$D$_5$H = 7.16 δ): δ = 5.68 (br s, 2H), 2.80 (br s, 1H), 2.09 (ABX m, ^2J = 16.4 Hz, ^3J = 5.6 Hz, ^3J = 8.0 Hz, 2H), 1.84 (d of unres m, 1H), 1.68 (s, 3H), 1.3−1.7 (m). [13]C + APT (75 MHz, C$_6$D$_6$, C$_6$D$_6$ = 128.3 δ): δ = 205.99 (up, C=O), 130.62 (down, CH=), 128.26 (down, CH=), 49.16 (up, CH$_2$), 39.65 (up), 32.33, 31.61 (down), 30.32, 29.19 (up), 27.61 (down, CH$_3$ of tBu). IR (neat): 1715. MS (high res EI): calcd for C$_{13}$H$_{22}$O 194.1671, found 194.1669.

cis-5-tert-Butylcyclohex-2-enol (25). The compound was prepared by a modified literature procedure.[77] To a magnetically stirred suspension of LiAlH$_4$ (320 mg, 8.4 mmol) in anhydrous ether (20 mL) was added dropwise 5-tert-butylcyclohex-2-enone (**24**) (912 mg, 6.0 mmol) in 3 mL of anhydrous ether at −70 °C. The cold bath was removed, and the mixture was stirred at room temperature for 30 min. Water (0.320 mL) was added very slowly dropwise with caution, then 10% NaOH (0.320 mL), followed by water (0.960 mL). The mixture was filtered and washed with ether many times, and the combined extracts were evaporated to give 863 mg of colorless oil (93% yield). ^{1}H NMR (300 MHz, CDCl$_3$, CHCl$_3$ = 7.26 δ): 5.78 (m, 1H), 5.65 (m, 1H), 5.28 (m, 1H), 2.13 (m, 1H), 2.0 (m, 1H), 1.8 (m, 1H), 1.6 (br), 1.4 (m, 1H), 1.07 (m, 1H), 0.873 (s, 9H).

cis-5-tert-Butylcyclohex-2-enyl Vinyl Ether (5). The compound was obtained by the same procedure as described above for its *trans*-isomer **3**. *cis*-5-tert-Butylcyclohex-2-enol (**25**)[77] (214 mg, 0.72 mmol), Hg(OAc)$_2$ (2 × 32 mg), ethyl vinyl ether (7 mL), and 20 h reflux gave a colorless oil after Kugelrohr distillation. ^{1}H NMR (300 MHz, concentrated in C$_6$D$_6$, C$_6$D$_5$H = 7.16 δ): δ = 6.34 (dd, $^3J_{cis}$ = 6.6 Hz, $^3J_{trans}$ = 14.1 Hz, 1H), 5.81 (dm, $^3J_{cis}$ = 9.0 Hz, J = 1.5 Hz, 1H), 5.61 (dm, J = 9 Hz, 2.5 Hz, 1H), 4.43 (dd, ^3J = 1.2 Hz, $^3J_{trans}$ = 14.1 Hz, 1H), 4.32 (fine m, 1H, CH−O), 4.05 (dd, ^2J = 1.5 Hz, $^3J_{cis}$ = 6.6 Hz, 1H), 2.06 (m, 1H), 1.67−1.79 (m, 1H), 1.50−1.62 (m, 1H), 1.27 (m, 1H), 1.16 (m, 1H), 0.71 (s, 9H). [13]C + APT (75 MHz, C$_6$D$_6$, C$_6$D$_6$ = 128.39 δ): δ = 150.71 (down, O−CH=), 130.33 (down, CH=), 128.44 (down, CH=), 88.58 (up, CH$_2$=), 76.71 (down, CH−OR), 43.33 (down, CH−t-Bu), 32.50 (up, C of t-Bu), 31.42 (up, CH$_2$), 27.41 (up, CH$_2$). 27.37 (down, CH$_3$ of t-Bu). MS (high res EI): calcd for C$_{12}$H$_{20}$O 180.1514, found 180.1509.

(cis-5-tert-Butylcyclohex-2-enyl)acetaldehyde (26). The solution of *cis*-5-tert-butylcyclohex-2-enyl vinyl ether (**5**) in benzene-d_6 was kept in a pressure/vacuum NMR tube at 180 °C for 5 h. ^{1}H NMR (300 MHz, C$_6$D$_6$, C$_6$D$_5$H = 7.16 δ): δ = 9.40 (t, J = 2.0 Hz, 1H), 5.61 (m, 1H), 5.38 (d of unres m, 1H), 2.47 (m, 1H), 2.92 (d of t, 1H), 1.82 (m, 1H), 1.67 (m, 1H), 1.57 (m, 1H), 1.23 (dd of t, 1H), 0.75 (s, 9H). [13]C + APT (75 MHz, C$_6$D$_6$, C$_6$D$_6$ = 128.39 δ): δ = 200.87 (down, CHO), 130.56 (down, CH=), 128.60 (down, CH=), 50.74 (up, CH$_2$), 44.63 (down, CH), 32.87 (down), 32.55 (up), 31.86 (up), 29.34 (down), 27.55 (down, Me), 27.34 (up). IR (neat): 3025, 2965, 2925, 2890, 2875, 2725, 1735. MS (high res EI): calcd for C$_{12}$H$_{20}$O 180.1514, found 180.1509.

2-Cyclohexenyl Vinyl Ether (6).[78] The compound was prepared from 2-cyclohexenol (800 mg), ethyl vinyl ether (17 mL), and Hg(OAc)$_2$ (2 × 60 mg) by the same procedure as described above for **3** and **5**. ^{1}H NMR (300 MHz, C$_6$D$_6$, C$_6$D$_5$H = 7.16 δ): δ = 6.28 (dd, 1H, J = 6.9, 14.4 Hz), 5.78 (m, 1H), 5.66 (m, 1H), 4.38 (dd, $^3J_{trans}$ = 14.4 Hz, ^2J = 1.5 Hz, 1H), 4.12 (unres m, 1H), 4.01 (dd, $^3J_{cis}$ = 6.6 Hz, ^2J = 1.5 Hz, 1H), 1.53−1.75 (m, 5H), 1.27 (m, 1H). [13]C + APT (75 MHz, C$_6$D$_6$, C$_6$D$_6$ = 128.39 δ): δ = 151.34 (down, O−CH=),

(114) Watanabe, W. H.; Conlon, L. E. *J. Am. Chem. Soc.* **1957**, *79*, 2828.
(115) Agosta, W. C.; Wolff, S. *J. Am. Chem. Soc.* **1976**, *98*, 4182−4188.

131.62 (down, CH=), 127.46 (down, CH=), 88.43 (up, CH$_2$=), 72.91 (down, CH−O), 29.13 (up, CH$_2$), 25.51 (up, CH$_2$), 19.67 (up, CH$_2$).

Cyclohex-2-enylacetaldehyde. The procedure was exactly the same as for the thermal rearrangement of **5** to **26**. ^{1}H NMR (300 MHz, C$_6$D$_6$, C$_6$D$_5$H = 7.16 δ): δ = 9.34 (t, J = 1.8 Hz, 1H), 5.57 (m, 1H), 5.38 (d of unres m, 1H), 2.40 (unres m, 1H), 0.95−1.90 (m, 8H). ^{13}C + APT (75 MHz, C$_6$D$_6$, C$_6$D$_6$ = 128.39 δ): δ = 200.81 (down, CHO), 130.78 (down, CH=), 128.43 (down, CH=), 50.40 (up, CH$_2$), 30.48 (down, CH), 29.47, 25.51, 21.64 (all up, 3 CH$_2$). IR (neat): 3025, 2965, 2930, 2860, 2845, 2725, 1735. MS (high res EI) calcd for C$_8$H$_{12}$O 124.0888, found 124.0884.

Supporting Information Available: Coordinates for optimized geometries, bond distances and angles, various energies, vibrational frequencies, and atomic charges for all structures treated (PDF). This material is available free of charge via the Internet at http:pubs.acs.org.